Available online at www.sciencedirect.com
ScienceDirect
Journal of the Franklin Institute 344 (2007) 312–348
Journal of The Franklin Institute
www.elsevier.com/locate/jfranklin

A review of computer-aided diagnosis of breast cancer: Toward the detection of subtle signs ☆

Rangaraj M. Rangayyan[a,b,*], Fábio J. Ayres[a], J.E. Leo Desautels[a,c]

[a]*Department of Electrical and Computer Engineering, Schulich School of Engineering, University of Calgary, Calgary, Alberta, Canada*
[b]*Department of Radiology, University of Calgary, Calgary, Alberta, Canada*
[c]*Alberta Cancer Board: Screen Test, Calgary, Alberta, Canada*

Received 13 March 2006; received in revised form 15 August 2006; accepted 1 September 2006

Abstract

Mammography is the best available tool for screening for the early detection of breast cancer. Mammographic screening has been shown to be effective in reducing breast cancer mortality rates: screening programs have reduced mortality rates by 30–70%.

Mammograms are difficult to interpret, especially in the screening context. The sensitivity of screening mammography is affected by image quality and the radiologist's level of expertise. Computer-aided diagnosis (CAD) technology can improve the performance of radiologists, by increasing sensitivity to rates comparable to those obtained by double reading, in a cost-effective manner. Current research is directed toward the development of digital imaging and image analysis systems that can detect mammographic features, classify them, and provide visual prompts to the radiologist.

Radiologists would like the ability to change the contrast of a mammogram, either manually or with pre-selected settings. Computer techniques for detecting, classifying, and annotating diagnostic features on the images would be desirable. This paper presents an overview of digital image processing and pattern analysis techniques to address several areas in CAD of breast cancer, including: contrast enhancement, detection and analysis of calcifications, detection and analysis of masses and tumors, analysis of bilateral asymmetry, and detection of architectural distortion. Although a few commercial CAD systems have been released, the detection of subtle signs of breast cancer such as global bilateral asymmetry and focal architectural distortion remains a difficult

☆A preliminary version of this paper was presented at The First World Experts' Congress on Women's Health Medicine and Healthcare, World Academy of Biomedical Technologies, Paris, France, March 2005.

*Corresponding author. Department of Electrical and Computer Engineering, Schulich School of Engineering, University of Calgary, Calgary, Alberta, Canada T2N 1N4.
E-mail addresses: ranga@ucalgary.ca (R.M. Rangayyan), fjayres@ucalgary.ca (F.J. Ayres).

0016-0032/$30.00
doi:10.1016/j.jfranklin.2006.09.003

problem. We present some of our recent works on the development of image processing and pattern analysis techniques for these applications.

Keywords: Breast cancer; Computer-aided diagnosis; Mammography; Calcifications; Breast masses; Breast tumors; Asymmetry; Architectural distortion; Enhancement; Segmentation

1. Screening for breast cancer

Breast cancer is the most frequently diagnosed cancer in women. According to the National Cancer Institute of Canada, the lifetime probability of developing breast cancer is one in 8.9, and the lifetime probability of death due to breast cancer is one in 26.8 [1]. Breast cancer has the highest prevalence among all cancers in the female population, with 1.0% of all women living with the disease [1].

Early detection of breast cancer is of utmost importance: localized cancer leads to a 5-year survival rate of 97.5%, whereas cancer that has spread to distant organs has a 5-year survival rate of only 20.4% [2]. Breast self-examination is not adequate: many studies indicate that there is no evidence of a reduction in the mortality rate due to breast cancer in women who practice regular breast self-examination, compared to those who do not [3,4].

Mammography is, at present, the best available examination for the detection of early signs of breast cancer [3]. It can reveal pronounced evidence of abnormality, such as masses and calcifications, as well as subtle signs such as bilateral asymmetry and architectural distortion [5]. Mammographic screening has been shown to be effective in reducing breast cancer mortality rates: screening programs have reduced mortality rates by 30–70% [6], [7, Chapter 19]. Cady and Chung [8] discuss the validity of mammographic screening programs, highlighting the reduction in mortality achieved by several screening programs in Sweden, the Netherlands, the UK, Finland, Italy, and the USA. The drawbacks of screening are also discussed, such as the higher incidence of unnecessary biopsies, cost and quality of interpretation of mammograms versus the experience of the radiologists, and the psychological consequences of errors, such as the anxiety caused by a false-positive result and the wrongful reassurance provided by a false-negative test. It has been concluded that the benefits of screening surpass the drawbacks, and that the practice of mammographic screening must be encouraged and expanded.

However, interpreting screening mammograms is not easy: the sensitivity of screening mammography is affected by image quality and the radiologist's level of expertise. Another factor that affects a radiologist's performance is the high volume of cases examined in a screening program. The lack of expert radiologists to analyze mammograms in remote or rural areas is also a matter of concern. Bird et al. [9] estimated the sensitivity of screening mammography to be between 85% and 90%. Misinterpretation of breast cancer signs accounted for 52% of the errors, and overlooking signs corresponded to 43% of the missed abnormalities. In a study by van Dijck et al. [10], minimal signs of abnormalities were found to be present on screening mammograms taken previously in many cases of screen-detected cancers. Double reading of screening mammograms was found to provide greater sensitivity than single reading without increasing recall rates, in a comparative analysis by Blanks et al. [11], but the manpower required may render such an approach impractical.

Among the most commonly missed signs of breast cancer is architectural distortion, which is defined in the Breast Imaging Reporting and Data System (BI-RADS) [12] as follows: "The normal architecture is distorted with no definite mass visible. This includes spiculations radiating from a point and focal retraction or distortion at the edge of the parenchyma". Sickles [13] reported that indirect signs of malignancy (such as architectural distortion, bilateral asymmetry, single dilated duct, and developing densities) accounted for almost 20% of the detected cancers. Burrell et al. [14] observed that architectural distortion was the most commonly missed abnormality in false-negative cases, in a study of cases of screening interval breast cancer.

2. Computer-aided diagnosis of breast cancer

Computer-aided diagnosis (CAD) techniques could offer a cost-effective alternative to double reading as a means of reducing errors. A CAD system could act as a second reader, prompting the radiologist to review areas in a mammogram deemed to be suspicious by specialized computer algorithms. A typical CAD session works as follows:

(1) The radiologist performs the first reading of the mammogram, recording any questionable or suspicious areas. Optionally, the radiologist could digitally enhance the mammographic image in order to pay closer attention to subtle details that could suggest the presence of lesions.
(2) The CAD system scans the mammogram in order to detect suspicious features.
(3) The radiologist then analyzes the prompts given by the CAD system to verify whether any suspicious area was left unchecked in the first reading.
(4) CAD algorithms may also be employed to estimate the likelihood that a given lesion is malignant or benign, with such an estimate reviewed subsequently by the radiologist.

The potential benefits of CAD technology motivated the development of several commercial CAD systems, such as the "ImageChecker" (R2 Technology, Sunnyvale, CA [15]) and "SecondLook" (iCAD, Nashua, NH [16]). These systems are under investigation regarding their benefits in a screening or diagnostic environment. Recent studies have demonstrated that CAD systems can improve a radiologist's sensitivity without a substantial increase in the recall rate [17].

Ciatto et al. [18] compared conventional mammogram reading and CAD reading on a national proficiency test of screening mammography in Italy. The authors concluded that the performance of single reading with CAD is similar to that of double reading. Freer and Ulissey [19] performed a prospective study of the effect of CAD in screening, where 12,860 screening mammograms were interpreted with the help of a CAD system over a 12-month period. It was observed that the number of cancers detected increased by 19.5%, and the proportion of early-stage malignancies detected increased from 73% to 78%. The recall rate increased from 6.5% to 7.7%, and the positive-predictive value of biopsy remained unchanged at 38%. The study led to the conclusion that CAD can improve the detection of early-stage malignancies without an excessively adverse effect on the recall rate or the positive-predictive value of biopsy.

Burhenne et al. [20] studied the performance of a commercial CAD system in the detection of masses and calcifications in screening mammography, obtaining a sensitivity of 75% in the detection of masses and architectural distortion, at one false positive per

image. Evans et al. [21] investigated the ability of a commercial CAD system to mark invasive lobular carcinoma of the breast: the system identified correctly 17 of 20 cases of architectural distortion. Birdwell et al. [22] evaluated the performance of a commercial CAD system in marking cancers that were overlooked by radiologists: the software detected five out of six cases of architectural distortion, and 77% of the previously missed lesions, at 2.9 false positives per image.

However, Baker et al. [23] found the sensitivity of two commercial CAD systems to be poor in detecting architectural distortion: fewer than 50% of the 45 cases of architectural distortion presented were detected (with a lower image-based sensitivity of 38%, or 30 out of 80 images, at 0.7 false positive per image). Broeders et al. [24] suggested that improvements in the detection of architectural distortion could lead to an effective improvement in the prognosis of breast cancer patients.

Table 1 presents a summary of the results obtained in the aforementioned studies. These findings indicate the need for further research in this area, and the development of

Table 1
Clinical evaluation of commercial CAD systems

Authors	Size of dataset	Summary of results
Ciatto et al. [18]	89 negative screening mammograms, plus 31 reported as negative and developing interval cancer in the following two-year interval (11 false negatives, 20 showing minimal signs), 19 radiologists	Double reading: sensitivity of 46.1% and recall rate of 26.1%. CAD reading: sensitivity of 42.1% and recall rate of 23.9%
Freer and Ulissey [19]	12,860 screening mammograms	Number of cancers detected increased by 19.5%; proportion of early-stage malignancies detected increased from 73% to 78%; recall rate increased from 6.5% to 7.7%; positive-predictive value of biopsy remained unchanged at 38%
Burhenne et al. [20]	1,083 (406 with calcifications, 677 with masses or architectural distortion), 20 radiologists	Sensitivity of 75% in the detection of masses and architectural distortion, at one false positive per image; sensitivity of 99% in the detection of microcalcifications; recall rates remained approximately unchanged (before installation of CAD system: 8.3%; after installation of CAD system: 7.6%)
Evans et al. [21]	90 mammograms (94 invasive lobular carcinoma lesions)	CAD detected 86 out of 94 lesions (sensitivity of 91%); detected 17 of 20 cases of architectural distortion (sensitivity of 85%)
Birdwell et al. [22]	110 cases of screen-detected cancers, where the prior mammograms were available, and where a panel of radiologists recommended a recall, on retrospective analysis	CAD marked 77% of the missed lesions, at 2.9 false positives per image
Baker et al. [23]	43 cases, 45 detected regions of architectural distortion	Fewer than 50% of the 45 cases of architectural distortion were detected; image-based sensitivity of 38%, or 30 out of 80 images, at 0.7 false positive per image

algorithms designed specifically to characterize architectural distortion. The remaining sections of this paper provide a review of several image analysis components of CAD systems and indicate the state-of-the-art as well as directions for the future.

3. Techniques for CAD of breast cancer

The development of new algorithms for CAD of breast cancer is an active research field [25,26], particularly in regards to the detection of subtle abnormalities in mammograms, and in spite of the success of a few commercial CAD systems in the improvement of the rates of detection of breast cancer. A substantial record of research exists in the literature regarding the detection and classification of masses and calcifications. These problems are generally considered to be well studied, and new developments must meet or exceed the high standards of performance set by the existing algorithms. Furthermore, commercial CAD systems have achieved a satisfactory degree of effectiveness in the detection of masses and calcifications. Nevertheless, certain areas of research in CAD of breast cancer still demand attention.

A relatively small number of researchers (as compared to the number of researchers who have conducted works related to masses and calcifications) have concentrated their attention on the problem of detecting architectural distortion in the absence of a central mass. Most of the published efforts are directed toward a more general category of abnormalities, such as spiculated lesions, which encompasses some of the possible appearances of architectural distortion. Other lines of research that require more attention include the analysis of bilateral asymmetry, curvilinear structures (CLS), and breast density as a predictor of the risk of breast cancer. In a larger context, areas of interest related to CAD of breast cancer include the development of systems for content-based retrieval of mammograms, indexed atlases, and data-mining systems. Full-field digital mammography systems, although still under evaluation, could facilitate the routine application of the techniques mentioned above.

3.1. Image enhancement

Diagnostic features in mammograms, such as masses and calcifications, may be small and have low contrast with respect to the surrounding breast tissues. These attributes could render the diagnostic features hard to detect. Contrast enhancement techniques can improve the ability of a radiologist to perceive subtle diagnostic features, leading to earlier, more accurate diagnosis of breast cancer. Contrast enhancement can improve the quality of an otherwise unsatisfactory mammogram, as stated by Ram [27], who further indicated that the application of contrast enhancement techniques in a clinical situation may reduce the radiation dose by about 50%. The enhancement of mammographic images could improve the accuracy of detection of early signs of breast cancer. For reviews on image enhancement in mammography, see Rangayyan [28], Morrow et al. [29], and Rangayyan et al. [30].

Traditional image enhancement techniques have been applied to radiography for more than three decades. Chan et al. [31] investigated the application of unsharp masking for digital mammography. Receiver operating characteristics (ROC) studies were conducted, and it was shown that unsharp masking improved the detectability of calcifications in digital mammograms. However, the method increased noise and caused some artifacts in the images.

Classical image enhancement techniques are often global transformations, i.e., techniques that do not adapt to the local information content in an image. There is significant variability in the size and shape of diagnostic features in mammograms, and classical techniques often perform poorly in enhancing various sections of a mammogram. Therefore, it is necessary to devise adaptive contrast enhancement algorithms for mammographic images, where the transformation is adapted to the local context of the given image. Laine et al. [32] presented a method for nonlinear contrast enhancement based on multi-resolution representation and the use of dyadic wavelets.

Gordon and Rangayyan [33] were the first to report on the use of adaptive-neighborhood image processing to enhance mammographic image contrast. Rangayyan and Nguyen [34] defined a tolerance-based method for growing foreground regions that could have arbitrary shapes rather than square shapes. Morrow et al. [29] further developed this approach with a new definition of background regions. The adaptive-neighborhood contrast enhancement (ANCE) algorithm works as follows: each pixel in the digitized mammographic image is taken as the seed pixel in a region growing procedure. The region growing procedure identifies the set of pixels that are similar and connected to the seed pixel (called the foreground region), as well as a three-pixel wide ribbon of pixels surrounding the foreground region (called the background region). The new value of the seed pixel in the contrast-enhanced image is determined by using the contrast value between the foreground and the background regions. Fig. 1 illustrates the result of the ANCE algorithm applied to a mammogram displaying a cluster of calcifications.

Dhawan et al. [35] investigated the benefits of various contrast transfer functions in a square-adaptive-neighborhood algorithm for contrast enhancement. The evaluated contrast transfer functions included $\ln(1+3C)$, $1-\exp(-3C)$, $\sqrt{C}$, and $\tanh(3C)$, where C is the original contrast. They found that while a suitable contrast function was important to bring out the features of interest in mammograms, it was difficult to select such a function. Dhawan and Le Royer [36] proposed a tunable contrast enhancement function for improved enhancement of mammographic features.

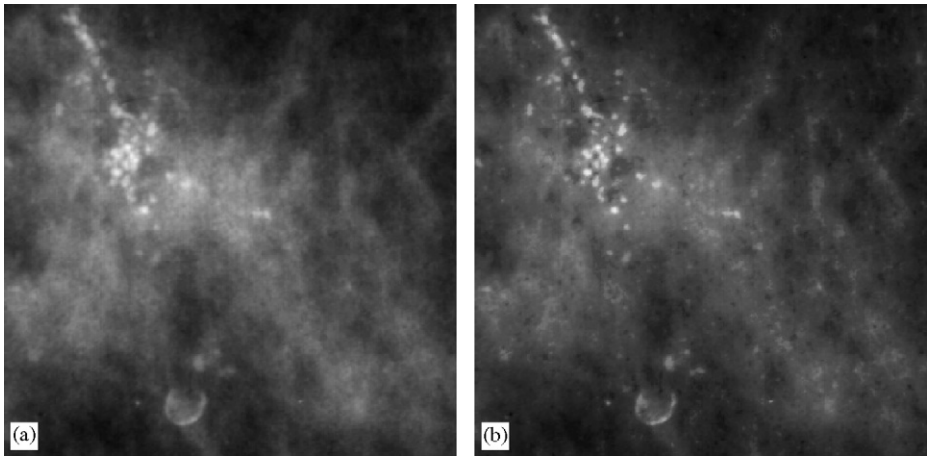

Fig. 1. (a) Part of a mammogram with a cluster of calcifications: true size 43×43 mm. (b) Result of adaptive-neighborhood contrast enhancement. Reproduced with permission from Morrow et al. [29] © IEEE.

It is important to distinguish between the effects of enhancement algorithms on the detection of the presence of features such as microcalcifications in an image, as against their effects on the diagnostic conclusion about a subject. Some image enhancement techniques may improve the visibility of diagnostic features, but distort their appearance and shape characteristics, possibly leading to misdiagnosis [37].

Rangayyan et al. [30,38] investigated the performance of their ANCE algorithm in increasing the sensitivity of breast cancer diagnosis by using ROC analysis and McNemar's tests [28]. A set of 78 screen-film mammograms of 21 difficult cases (14 malignant and seven benign) and another set of 222 screen-film mammograms of 28 interval cancer patients and six benign control cases were digitized with a resolution of about $4096 \times 2048 \times 10$-bit pixels, and subsequently processed with the ANCE algorithm. The original films, as well as the corresponding unprocessed and processed digital images, were presented to six experienced radiologists for an ROC analysis of the difficult-case set, and to three radiologists for analysis of the interval-cancer set. It was observed that the radiologists' performance improved with ANCE processing, with respect to both film and digital image reading, in terms of the area under the ROC curve. It was also observed that the diagnostic sensitivity was improved by the ANCE algorithm. McNemar's tests of symmetry indicated that the diagnostic confidence for the interval-cancer cases was improved by the ANCE technique with a high level of statistical significance ($p = 0.0001$–0.005), with no significant effect on the diagnosis of the benign control cases (p-values of 0.08–0.1).

Sivaramakrishna et al. [39] compared the performance of several contrast enhancement algorithms in a preference study. The compared algorithms were: ANCE [29], adaptive unsharp masking [40], contrast-limited adaptive histogram equalization [41], and wavelet-based enhancement [42]. In a majority of the cases with microcalcifications, the ANCE algorithm provided the most-preferred images. In the case of images with masses, the unenhanced (original) images were preferred in most of the cases.

Many methods for the enhancement of mammograms may cause an amplification of noise or distortion of the anatomical features present in the image. Radiologists would prefer to have the enhanced image maintain the familiar appearance of the original mammogram, which may limit the scope of enhancement techniques. However, with the introduction of direct digital imaging systems to mammography (with increased contrast, dynamic range, and signal-to-noise ratio [SNR]), there may no longer remain the need to enhance the image.

3.2. Segmentation of mammograms and analysis of breast density

It has been observed that increased breast density is generally associated with a higher risk of development of cancer [43,44]. Many researchers have investigated computer methods for the assessment of the risk of development of breast cancer via automated analysis of breast density. Byng et al. [45] computed the skewness of histograms of 24×24 (3.12×3.12 mm) sections of mammograms. An average skewness was computed for each image by averaging over all the section-based skewness measures of the image. Mammograms of breasts with increased fibroglandular density were observed to have histograms skewed toward higher density, resulting in negative skewness. On the other hand, mammograms of fatty breasts tended to have positive skewness. The fractal dimension of the breast image was also computed: the image was interpreted as a relief

map and the fractal dimension was computed using the box-counting method. The skewness and the fractal dimension measures were found to be useful in predicting the risk of development of breast cancer.

Caulkin et al. [46] observed that breast cancer occurs more frequently in the upper and outer quadrants of the breast, and that the majority of cancers are associated with glandular rather than fatty tissues. Therefore, the detection of different anatomical structures in the breast (such as fatty tissue, the fibroglandular disk, and the pectoral muscle), could facilitate the analysis of the risk of development of breast cancer, as well as the detection of early breast cancer. However, most of the proposed techniques for CAD of breast cancer analyze the whole mammogram, without considering the observation that signs of breast cancer may have different appearances in different regions. Based upon these observations, some researchers have proposed methods to segment and also to model mammograms in terms of anatomical regions.

Karssemeijer [47] used the Hough transform to identify the pectoral muscle as a straight-line edge in the mammogram. Ferrari et al. [48] proposed two methods for the identification of the pectoral muscle in mammograms. The first method is a variant of Karssemeijer's method, which employs the Hough transform and filtering applied to the accumulator cells. However, the hypothesis of a straight line for the representation of the pectoral muscle is not always valid, and may impose limitations on subsequent stages of image analysis. The second method proposed by Ferrari et al. [48], based upon directional filtering using Gabor wavelets, overcomes this limitation.

Saha et al. [49] employed scale-based fuzzy connectivity methods to segment dense regions from fatty regions in mammograms. The segmented dense and fatty regions were quantified by measuring the respective area and total density, and a set of features was derived from these measures. The features were linearly correlated between the medio-lateral oblique (MLO) and the cranio-caudal (CC) views in order to demonstrate the inter-view similarity. The precision in the segmentation was measured by comparing the automatically segmented contours of the dense regions with manually delineated references drawn by experienced radiologists. The method was tested on 60 cases, each case including the MLO and CC projections. The method was found to be robust in the segmentation of dense regions, and the authors observed the density features to be strongly correlated between the MLO and CC views.

Several authors have reported on techniques for the delineation of the breast boundary [50]. Ferrari et al. [51] developed a method for the identification of the breast boundary using active contour models, in which the mammogram is first contrast-enhanced and thresholded, producing an initial chain-code representation of the breast boundary. The final boundary is obtained by the application of a specially tailored active contour model algorithm. The method was applied to 84 MLO mammograms from the Mini-MIAS database. The evaluation of the breast contours obtained by this method was performed based upon the percentage of false-positive and false-negative pixels, in comparison to contours that were manually drawn by a radiologist. The average false-positive and false-negative rates were 0.41% and 0.58%, respectively.

Ferrari et al. [52] proposed a method to segment the fibroglandular disk in mammograms based upon the Gaussian mixture model. In this method, prior to the detection of the fibroglandular disk, the breast boundary and the pectoral muscle are detected using other methods developed by the authors [48,51] (mentioned above). The fibroglandular disk is detected by defining a breast density model. The parameters of

the model are estimated using the expectation-maximization algorithm and the minimum-description-length principle. A qualitative assessment of the segmentation results, performed by an experienced radiologist, resulted in 64.3% of the results being rated as excellent, 16.7% rated as good, 10.7% rated as average, 4.7% rated as poor, and only 3.6% of the results as failed segmentation.

Methods for the analysis of breast density should incorporate prior segmentation and removal of the pectoral muscle from mammograms (MLO views) as well as the detection of the breast boundary and removal of artifacts outside the breast region in mammograms. Delineation of the fibroglandular disk and statistical representation of the various types of tissue within the breast using a Gaussian mixture model [52] should be employed to improve the accuracy and extend the scope of analysis of breast density. Selective analysis of breast density could lead to improvements in the prediction of the risk of development of breast cancer based upon screening mammograms.

3.3. Detection and classification of microcalcifications

Calcifications in mammograms appear as relatively bright regions due to the higher X-ray attenuation coefficient (or density) of calcium as compared with normal breast tissue. Calcifications present within dense masses or superimposed by dense tissues in the process of acquisition of mammograms could present low gray-level differences or contrast with respect to their local background. On the other hand, calcifications present against a background of fat or low-density tissue would possess higher differences and contrast. Malignant calcifications tend to be numerous, clustered, small, varying in size and shape, angular, irregularly shaped, and branching in orientation [53,54]. On the other hand, calcifications associated with benign diseases are generally larger, more rounded, smaller in number, more diffusely distributed, and more homogeneous in size and shape.

The detection and classification of microcalcifications has been extensively studied, with many authors reporting on several successful approaches to this task. A recent survey by Cheng et al. [55] lists almost 200 references on computer-aided detection and classification of microcalcifications, including methods for the visual enhancement of microcalcifications, segmentation, detection, analysis of malignancy, and strategies for the evaluation of detection algorithms.

Shen et al. [56] proposed a method for the detection and classification of mammographic calcifications. The method starts with a multi-tolerance region growing procedure for the detection of potential calcification regions and the extraction of contours. Shape features based on central moments, Fourier descriptors, and compactness are then extracted. Finally, a neural network is used for the classification of the feature vectors in order to distinguish between malignant and benign calcifications. The correct classification rates for benign and malignant calcifications were 94% and 87%, respectively [56]. In a related work [57] on the investigation of shape features and a more extensive analysis of classification of calcifications, a classification accuracy of 100% was obtained for both benign and malignant calcifications with a database containing 143 biopsy-proven calcifications (79 malignant and 64 benign).

Bankman et al. [58] reported on the use of a region-growing-based algorithm for the segmentation of calcifications that did not require threshold or window selection, and compared their algorithm to the aforementioned multi-tolerance method of Shen et al. as

well as to an active contours method. A theoretical analysis of the computational complexity of each method was presented, along with computer execution times for comparison. The authors found that all of the three methods had similar statistical performance; however, their own algorithm outperformed the other methods in terms of computational effort.

Strickland [59] developed a two-stage method based on wavelet transforms for the detection and segmentation of microcalcifications. In this method, the detection of calcifications is performed in the wavelet domain. The detected sites are enhanced in the wavelet domain, prior to the computation of the inverse wavelet transform. The appearance of microcalcifications is enhanced by this procedure; a threshold procedure suffices to segment the calcifications. The test database consisted of 40 mammograms, and a sensitivity of 91% at three false positives per image was obtained.

El-Naqa et al. [60] used support vector machines to detect microcalcification clusters. The algorithm was tested using 76 mammograms, containing 1120 microcalcifications. A sensitivity of 94% was reported, at one false positive per image. An improvement of the method was published by Wei et al. [61] using a relevance vector machine. A database of 141 mammograms containing microcalcifications was used to test the algorithm. The method achieved a sensitivity of 90% at one false positive per image. The statistical performance of the method was similar to that of the method of El-Naqa et al. [60], but the authors reported a 35-fold improvement in computational speed.

Yu et al. [62] used a wavelet filter for the detection of microcalcifications, and a Markov random field model to obtain textural features from the neighborhood of every detected calcification. The Markov-random-field-based textural features, along with three auxiliary textural features (the mean pixel value, the gray-level variance, and a measure of edge density), were used to reject false positives. The method was evaluated using 20 mammograms containing 25 areas of clustered microcalcifications. A sensitivity of 92% was obtained, at 0.75 false positive per image.

Yu and Guan [63] developed a technique for the detection of clustered microcalcifications that is comprised of two parts: detection of potential microcalcification pixels, and delineation of individual microcalcifications by the elimination of false positives. The first part involves the extraction of features based on wavelet decomposition and gray-level statistics, followed by a neural-network classifier. The detection of individual objects requires a vector of 31 features related to gray-level statistics and shape factors, followed by a second neural-network classifier. A database of 40 mammograms containing 105 clusters of calcifications was used to assess the performance of the proposed algorithm: a sensitivity of 90% was attained with 0.5 false positive per image.

Soltanian-Zadeh et al. [64] compared four groups of features according to their discriminant power in separating microcalcifications into the benign and malignant categories. The microcalcifications were segmented using an automated method, and several features were extracted. Each feature belonged to one of the following four categories: multi-wavelet-based features, wavelet-based features, Haralick's texture features [65], and shape features. Within each group, a feature-selection procedure based on genetic algorithms was employed to identify the most-suitable features for use with a k-nearest-neighbor classification scheme. The classification performance of each group of features was then determined using ROC analysis. The area under the ROC curve obtained ranged from 0.84 to 0.89, and it was observed that the multi-wavelet features yielded the best performance, followed by the shape features.

Serrano et al. [66] and Acha et al. [67] proposed a method for the detection of calcifications based upon the error of a 2D adaptive linear prediction algorithm [68] applied to the mammographic image. The method is based upon the observation that a microcalcification can be seen as a point of nonstationarity in an approximately homogeneous region or neighborhood in a mammogram; such a pixel cannot be predicted well by the linear predictor, and hence leads to a high error. The algorithm detects and localizes calcifications, and a multi-tolerance region growing algorithm [56] is employed to delineate each calcification. The results of this procedure are illustrated in Fig. 2 for a part of a mammogram with calcifications. It can be observed that the calcifications are correctly delineated in Fig. 2c, despite the poor contrast between the calcifications and the dense breast tissue in the background.

A summary of the statistical performance of selected CAD methods for the detection and classification of calcifications is provided in Table 2. Given the high levels of sensitivity in the detection of calcifications that have been achieved at low rates of false positives, this problem could be considered to be satisfactorily solved.

3.4. Detection and classification of masses

Breast tumors and masses usually appear in the form of dense regions in mammograms. A typical benign mass has a round, smooth, and well-circumscribed boundary; on the other hand, a malignant tumor usually has a spiculated, rough, and blurry boundary [5,12]. However, there do exist atypical cases of macrolobulated or spiculated benign masses, as well as microlobulated or well-circumscribed malignant tumors. Several techniques have been developed for the detection and classification of breast masses in mammograms. The commercial systems available at present incorporate some of these techniques, and there is mounting evidence in the scientific literature that such systems perform adequately.

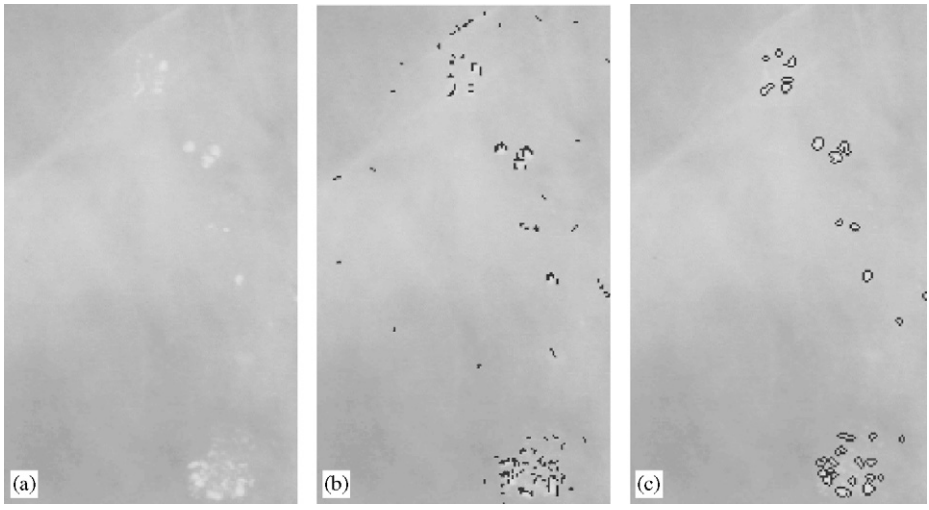

Fig. 2. (a) Mammogram section with malignant calcifications: 234×137 pixels with a resolution of 160 μm. (b) Seed pixels detected by thresholding the prediction error (marked in black). (c) Contours of the calcification regions detected by region growing from the seed pixels in (b). Reproduced with permission from Serrano et al. [66] © Cuban Society of Bioengineering.

Table 2
Performance statistics of selected CAD methods for the detection and classification of calcifications

Authors	Size of dataset	Summary of results
Shen et al. [56]	Four images, 58 benign calcifications, 241 malignant calcifications	Correctly classified 94% of the benign calcifications and 97% of the malignant calcifications
Shen et al. [57]	18 images, 79 malignant calcifications, and 64 benign calcifications	Classification accuracy of 100% for both benign and malignant calcifications
Bankman et al. [58]	Six images, 124 microcalcifications, and 2, 212 background structures	$A_z = 0.9$
Strickland [59]	40 mammograms	Sensitivity of 91% at three false positives per image
El-Naqa et al. [60]	76 mammograms containing 1, 120 microcalcifications	Sensitivity of 94% at one false positive per image
Wei et al. [61]	141 mammograms containing microcalcifications	Sensitivity of 90% at one false positive per image
Yu et al. [62]	20 mammograms containing 25 areas of clustered microcalcification	Sensitivity of 92% at 0.75 false positive per image
Yu and Guan [63]	40 mammograms, 105 clusters of microcalcifications	Detection rate of 90% with 0.5 false positive per image. Note: 20 training samples were also used in the testing step.
Soltanian-Zadeh et al. [64]	103 regions containing microcalcification clusters	$A_z = 0.89$
Serrano et al. [66]	428 microcalcifications	Detected 86% of the microcalcifications, with eight false detections

Only works with ROC analysis and/or pattern classification results are listed. A_z: area under the ROC curve.

Brzakovic et al. [69] reported on the use of a fuzzy pyramid linking technique for mass localization and shape analysis for false-positive elimination. Evaluation of the method was carried out on a small database of 25 mammographic images, leading to a classification accuracy of 85%.

Kegelmeyer et al. [70] proposed an algorithm for the detection of spiculated lesions that employed four Laws texture measures [71] and a new feature sensitive to stellate patterns. The test database consisted of 85 cases, with 49 normal cases and 36 positive cases; a total of 330 mammograms were used, with 68 lesions. A sensitivity of 97% was achieved at 0.28 false positive per image.

Karssemeijer and te Brake [72] developed a method for the detection of stellate patterns in mammograms, based on a statistical analysis of a map of the texture orientation in the mammographic images. The method for texture orientation analysis employs a multi-scale technique, and the orientation map is analyzed through the use of operators sensitive to stellate patterns. A sensitivity of 90% with one false positive per image was obtained in the detection of malignant stellate lesions and architectural distortion, using 31 normal cases and 19 cases with stellate lesions from the MIAS database [73] (website: http://www.wiau.man.ac.uk/services/MIAS/MIASweb.html). In a related work, te Brake and Karssemeijer [74] presented an algorithm for the identification of masses that is an extension of their previous work on the detection of stellate patterns. The mass-detection algorithm identifies patterns of radial gradient vectors, rather than radial spiculations.

A sensitivity of 75% was attained with one false positive per image, with a test database of 71 cases (132 mammograms) containing malignant tumors.

Rangayyan et al. [75] introduced two new shape factors, spiculation index and fractional concavity (see Fig. 3b), and applied them for the classification of manually segmented mammographic masses. The combined use of the spiculation index, fractional concavity, and compactness yielded a benign-versus-malignant classification accuracy of 81.5%.

Sahiner et al. [76,77] defined a "rubber-band straightening transform" (RBST) to map ribbons around breast masses in mammograms into rectangular arrays, and then computed Haralick's measures of texture [65]. The boundaries of 249 mammographic masses were automatically extracted. Haralick's texture measures individually provided classification accuracies of up to only 0.66, whereas the Fourier-descriptor-based shape factor defined by Shen et al. [57] gave an accuracy of 0.82 (the highest among 13 shape

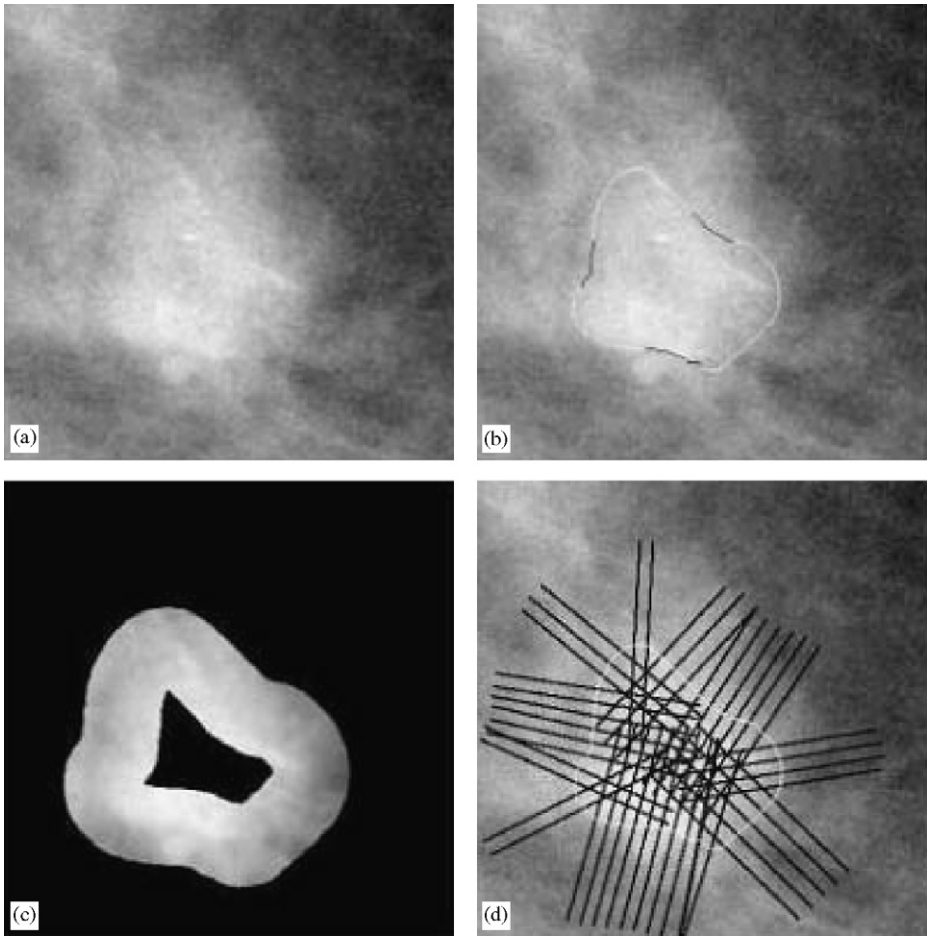

Fig. 3. (a) ROI of a benign mass. (b) ROI overlaid with the contour, demonstrating concave parts in black and convex parts in white. (c) Ribbon of pixels for the purpose of computing texture measures, derived by dilating and eroding the contour in (b). (d) Normals to the contour, shown at every 10th point on the contour, used for the computation of edge-sharpness measures. Reproduced with permission from Alto et al. [126] © SPIE and IS&T.

features, 13 texture features, and five run-length statistics). Each texture feature was computed using the RBST method [77] in four directions and for 10 distances. The full set of the shape factors provided an average accuracy of 0.85, the texture feature set provided the same accuracy, and the combination of shape and texture feature sets provided an improved accuracy of 0.89. These results indicate the importance of including features from a variety of perspectives and image characteristics in pattern classification.

Mudigonda et al. [78] computed Haralick's texture measures using adaptive ribbons of pixels extracted around mammographic masses (see Fig. 3c), and used the features to distinguish malignant tumors from benign masses using linear discriminant analysis. The method was tested on a database of 39 mammographic images, including 16 circumscribed benign, four circumscribed malignant, 12 spiculated benign, and seven spiculated malignant masses. The authors reported a classification accuracy of 74.4% with an area under the ROC curve of $A_z = 0.67$. It was observed that restricting feature extraction to ribbons around the contours of masses improved the classification accuracy as compared to extracting the features over the entire regions of the masses.

Mudigonda et al. [79] also proposed a method for the detection of masses in mammographic images based on the analysis of iso-intensity contour groups, and subsequent inspection of texture flow-field information to eliminate false positives. The test dataset consisted of 56 images from the Mini-MIAS database [73] including 30 benign lesions, 13 malignant cases, and 13 normals. The authors reported a sensitivity of 81% at 2.2 false positives per image. Fig. 4 illustrates the results of the procedure applied to a region of interest (ROI) of a mammogram containing two circumscribed benign masses. The method was also applied to the detection of masses in full mammographic images: the results are illustrated in Fig. 5 for a mammogram with a malignant tumor.

Rangayyan et al. [80] proposed the use of shape factors and edge acutance (see Fig. 3d) for the classification of manually segmented masses as benign or malignant, and spiculated or circumscribed. An overall classification accuracy of 95% was obtained with a database of 54 mammographic images, including 16 circumscribed benign, seven circumscribed malignant, 12 spiculated benign, and 19 spiculated malignant masses.

Li et al. [81] proposed a method for mass detection that employs a directional wavelet transform for multi-scale representation of the mammographic image, followed by segmentation of the mass at different scales, and the elimination of false-positive segments using shape analysis. A sensitivity of 91% with 3.2 false positives per image was obtained in the training phase of the proposed algorithm. The trained algorithm identified six of 10 subtle masses in a subsequent testing phase.

Zheng and Chan [82] devised an algorithm for the detection of masses that combines localized fractal analysis for pre-selection of suspicious regions, a multi-resolution Markov random field segmentation algorithm, and shape-based classification of segmented regions for reducing the number of false positives. The algorithm was evaluated using all of the 322 images in the Mini-MIAS database [73], and a sensitivity of 97.3% with 3.9 false positives per image was reported.

Liu et al. [83] formulated a multi-resolution procedure for the detection of spiculated lesions in digital mammograms. A multi-resolution representation of the mammographic image was obtained using a linear-phase, nonseparable, 2-D wavelet transform. Pixel-based features were extracted at each resolution level, and the resulting feature maps were

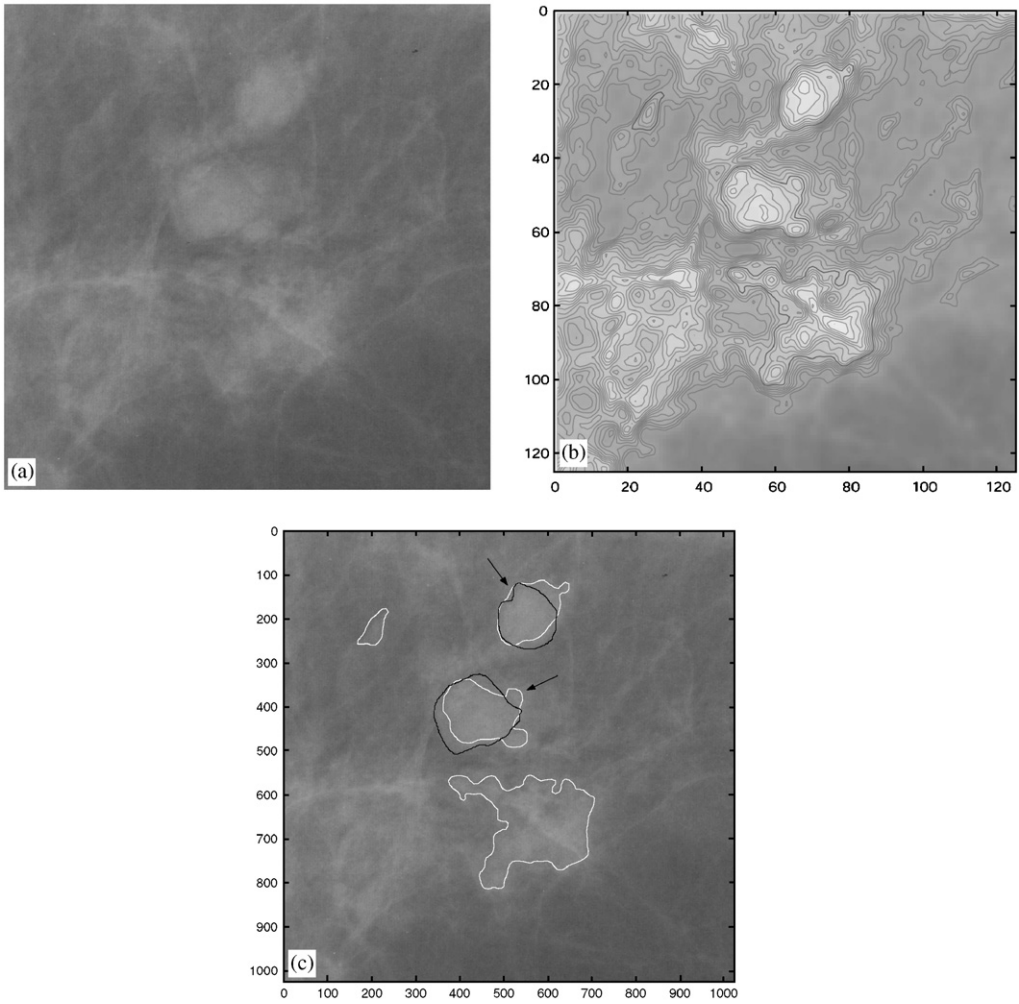

Fig. 4. (a) A 1024×1024 section of a mammogram containing two circumscribed benign masses. Pixel size $= 50\,\mu m$. Image width $= 51$ mm. (b) Groups of iso-intensity contours in the third multi-resolution version of the image in (a). (c) The contours (white) of two masses (indicated by arrows) and two false positives detected, with the corresponding contours (black) of the masses drawn independently by a radiologist. Reproduced with permission from N.R. Mudigonda, R.M. Rangayyan and J.E.L. Desautels, "Segmentation and classification of mammographic masses", *Proceedings of SPIE Volume 3979, Medical Imaging 2000: Image Processing,* pp. 55–67, 2000. © SPIE.

analyzed, from the coarsest to the finest resolution, to determine the sites of spiculated lesions. The algorithm was tested using a database of 19 spiculated lesions and 19 normal mammograms from the MIAS database, and a sensitivity of 100% with 2.2 false positives per image was reported.

Zwiggelaar et al. [84] introduced a technique to detect abnormal patterns of linear structures by detecting the radiating pattern of linear structures and/or the central mass expected to occur with spiculated lesions. Principal component analysis (PCA) was applied

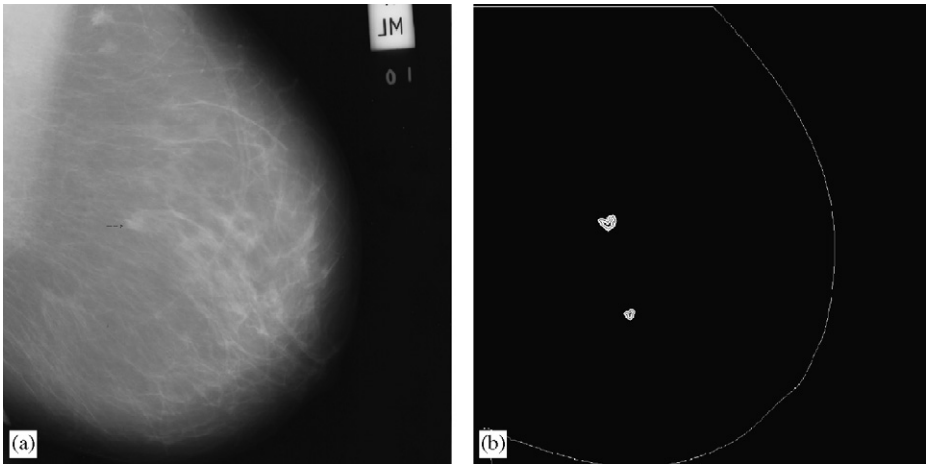

Fig. 5. (a) A mammogram (size 1024×1024 pixels, 200 μm per pixel) with a spiculated malignant tumor (pointed by the arrow, radius = 0.54 cm). Case mdb144 from the MIAS database [73]. (b) Adaptive ribbons of pixels (white) and boundaries (black) of the regions retained in the mammogram after the false-positive analysis stage. The larger region corresponds to the malignant tumor; the other region is a false positive. Reproduced with permission from N.R. Mudigonda et al. [79] © IEEE.

to a training set of mammograms including normal tissue patterns and spiculated lesions. The results of PCA were used to construct a basis set of oriented texture patterns, which was used to analyze radiating structures. A sensitivity of 80% was obtained at 0.23 false positive per image.

Guliato et al. [85] devised two methods for the segmentation of masses using fuzzy sets. The first method determines the boundary of a mass by region growing, after a fuzzy-set-based preprocessing enhancement step; the method yielded tumor boundaries that were consistent with manually drawn contours. The second method incorporates the fuzzy-set theory into the region-growing procedure, producing a fuzzy segmentation of the masses. The authors observed that the degree of inhomogeneity around the mass boundary correlated with the benign/malignant nature of the tumor, because malignant tumors are expected to have ill-defined margins. Using a measure of inhomogeneity of the fuzzy segmentation in the boundary region, the authors obtained a benign/malignant classification sensitivity of 80% with a specificity of 90%. Guliato et al. [86] also developed a method for combining multiple segmentation results into a single result, using fuzzy fusion operators. The resulting segmentated regions were observed to be more consistent with the corresponding regions segmented by a radiologist than the individual results of segmentation.

Table 3 presents a summary of the statistical performance of selected methods for the detection and classification of masses. Although several methods have demonstrated good sensitivity above 85%, the accompanying false-positive rates are considered to be high. There is a need to increase the sensitivity of detection of masses to higher values around 95% at low false-positive rates of less than one per image. It is also desirable to indicate the degree of suspicion or probability of malignancy for each region identified.

Table 3
Performance statistics of selected CAD methods for the detection and classification of masses

Authors	Size of Dataset	Summary of Results
Brzakovic et al. [69]	25 mammograms	Classification accuracy of 85%
Kegelmeyer et al. [70]	85 cases (49 normals, 36 positives), 330 mammograms	Sensitivity of 97% at 0.28 false positive per image in the detection of spiculated lesions
Karssemeijer and te Brake [72]	31 normal mammograms, 19 mammograms with stellate lesions	Sensitivity of 90% with one false positive per image
te Brake and Karssemeijer [74]	71 cases (132 mammograms) containing malignant tumors	Sensitivity of 75% with one false positive per image
Rangayyan et al. [75]	manually segmented mammographic masses (boundaries of 28 benign masses and 26 malignant tumors)	Benign/malignant classification accuracy of 82%, $A_z = 0.79$
Sahiner et al. [76,77]	249 automatically segmented mammographic masses	Benign/malignant classification accuracy of 89%
Mudigonda et al. [78]	39 mammographic images (16 circumscribed benign, four circumscribed malignant, 12 spiculated benign, and seven spiculated malignant masses)	Classification accuracy of 74.4%, $A_z = 0.67$
Mudigonda et al. [79]	56 mammographic images (30 benign lesions, 13 malignant cases, and 13 normals)	Sensitivity of 81% at 2.2 false positives per image
Rangayyan et al. [80]	54 mammographic images (16 circumscribed benign, seven circumscribed malignant, 12 spiculated benign, and 19 spiculated malignant masses)	Benign/malignant and spiculated/circumscribed classification accuracy of 95%
Li et al. [81]	Training data set includes 36 normal and 24 abnormal mammograms (34 masses), testing data set includes 24 normal and 10 abnormal mammograms (10 masses)	Sensitivity of 91% with 3.21 false positives per image
Zheng and Chan [82]	All 322 images in the Mini-MIAS database [73]	Sensitivity of 97.3% with 3.9 false positives per image
Liu et al. [83]	19 mammograms exhibiting spiculated lesions, 19 normal mammograms	Sensitivity of 100% with 2.2 false positives per image
Zwiggelaar et al. [84]	56 mammograms (28 mammograms containing a spiculated lesion, 28 mammograms without an abnormality)	Sensitivity of 80% at 0.23 false positive per image
Guliato et al. [85]	47 mammograms (22 benign masses, 25 malignant tumors)	Benign/malignant classification sensitivity of 80% with a specificity of 90%

Only works with ROC analysis and/or pattern classification results are listed.

3.5. Analysis of CLS

The presence of CLS is an important factor in the detection of abnormalities in mammograms. The breast contains many structures that correspond mammographically to CLS, such as milk ducts, blood vessels, ligaments, parenchymal tissue, and edges of the pectoral muscle. Some lesions are characterized by the presence of certain types of CLS, such as spicules, in the mammographic image (for example, spiculated masses and architectural distortion), or by the asymmetric disposition of the oriented texture in the

breast image. Conversely, some lesions, such as circumscribed masses, may be obscured by superimposed CLS; the resulting altered appearance could lead to misdiagnosis. Therefore, the ability to detect and classify CLS could enhance the performance of CAD algorithms.

Evans et al. [87] developed a method for statistical characterization of normal CLS in mammograms. CLS were detected automatically, and six shape features were computed from each CLS. PCA was performed, and the two major dimensions were modeled using a Gaussian mixture model.

Wai et al. [88] proposed a method for the segmentation of CLS based on physical modeling of CLS in the breast. Qualitative experiments were conducted, and the authors reported that their method produced well-localized responses that are robust to the presence of noise.

Zwiggelaar et al. [89] investigated the performance of different methods for the detection and classification of CLS in mammograms, including: a line operator [90], orientated bins [91], steerable filters [92], and ridge detectors [93]. It was observed that the best method for CLS detection (line operator) yielded an area under the ROC curve of $A_z = 0.94$. Cross-sectional analysis of the detected profiles was performed, using PCA for dimensionality reduction, resulting in satisfactory discrimination between spicules and ducts ($A_z = 0.75$).

The pre-selection of CLS has been shown to lead to increased accuracy of detection of signs of breast cancer, such as spiculated tumors [72] and architectural distortion [94]. The few methods that have been proposed in the literature for the detection of CLS have demonstrated limited success. There exists the need for the development of improved detection and analysis techniques for accurate discrimination of spicules against blood vessels and ducts.

3.6. Analysis of bilateral asymmetry

One of the cues used by radiologists to detect the presence of breast cancer is bilateral asymmetry, where the left and right breasts differ from each other in overall appearance in the corresponding mammographic images. The BI-RADS [12] definition of asymmetry indicates the presence of greater volume or density of breast tissue without a distinct mass, or more prominent ducts, in one breast as compared to the corresponding area in the other breast.

Miller and Astley [95] proposed a technique for the detection of bilateral asymmetry that comprised a semi-automated texture-based procedure for the segmentation of the glandular tissue, and measures of shape and registration cost between views for detection of the occurrence of asymmetry. An accuracy of 86.7% was reported, on a test dataset of 30 screening mammogram pairs. In another report, Miller and Astley [96] presented a method for the detection of bilateral asymmetry based on measures of shape, topology, and distribution of brightness in the fibroglandular disk. The method was tested on 104 mammogram pairs, and a classification accuracy of 74% was obtained. Lau and Bischof [97] devised a method for the detection of breast tumors, using a localized definition of asymmetry that encompassed measures of brightness, roughness, and directionality. The method was evaluated using 10 pairs of mammograms where asymmetry was a significant factor in the radiologist's diagnosis. A sensitivity of 92% was obtained with 4.9 false positives per mammogram.

Ferrari et al. [98] developed a method for the analysis of asymmetry in mammograms using directional filtering with Gabor wavelets. In their method, the fibroglandular disk is segmented (Fig. 6 illustrates this step of the method), and the resulting image is

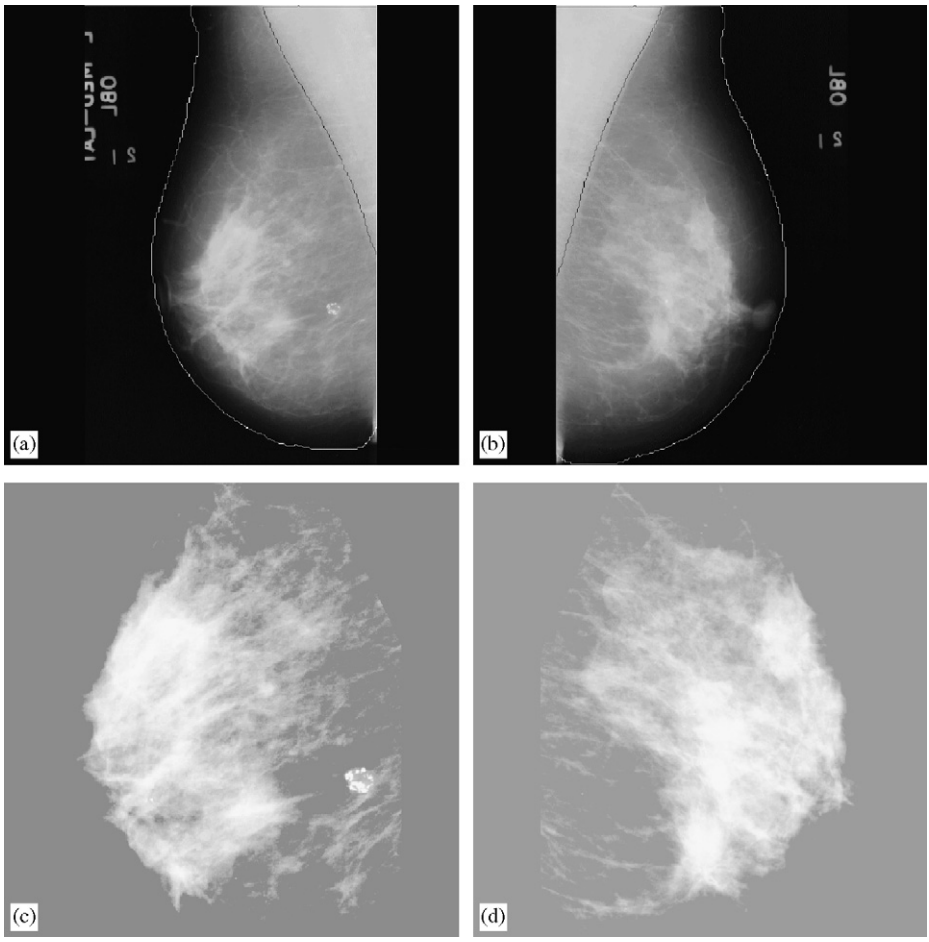

Fig. 6. Images mdb119 and mdb120 of a case of architectural distortion [73]. (a) and (b) Original images (1024×1024 pixels at 200 μm/pixel). The breast boundary (white) and pectoral muscle edge (black) detected are shown. (c) and (d) Fibro glandular disks segmented and enlarged (512×512 pixels). Histogram equalization was applied to enhance the global contrast of each ROI for display purposes only. Reproduced with permission from Ferrari et al. [98] © IEEE.

decomposed using a bank of Gabor filters at different orientations and scales. The Karhunen–Loève transform is employed to select the principal components of the filter responses. Rose diagrams are computed from the phase images, and subsequently analyzed to detect the presence of asymmetry as characterized by variations in oriented textural patterns (see Fig. 7). A database of 80 images from the Mini-MIAS database containing 20 normal cases, 14 asymmetric cases, and six architectural distortion cases was used to evaluate the algorithm. The authors reported classification accuracy rates of up to 74.4%. The Gabor-filter-based method gives quantitative measures of the differences in the directional distribution of the fibroglandular tissue (pattern asymmetry). Rangayyan et al. [99] extended the method of Ferrari et al. [98] by including morphological measures quantifying differences in fibroglandular-tissue-covered area in the left and right breasts,

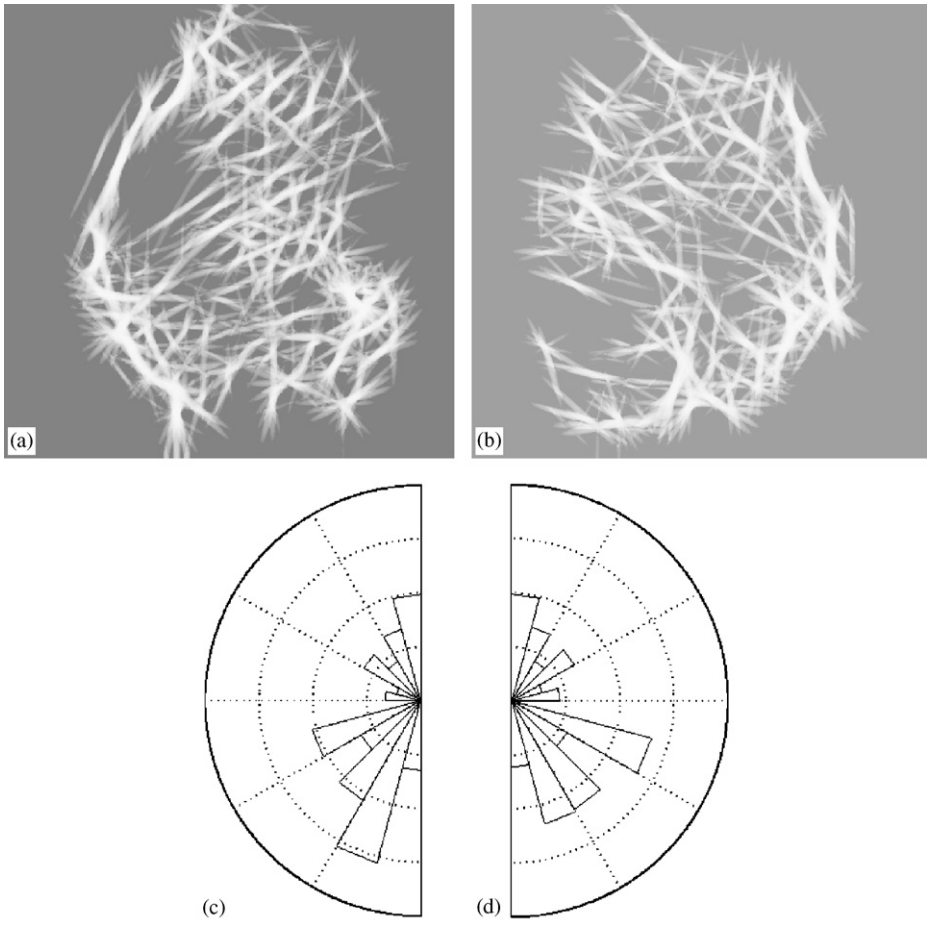

Fig. 7. Results of analysis of bilateral asymmetry for the case of architectural distortion in Fig. 6. (a) and (b) Magnitude images. (c) and (d) Rose diagrams. The magnitude images were histogram-equalized for improved visualization. The rose diagrams have been configured to match the mammograms in orientation. Reproduced with permission from Ferrari et al. [98] © IEEE.

which relate to size and shape; in addition, the directional data were aligned with reference to the edge of the pectoral muscle (in MLO views). A sensitivity of 82.6% and a specificity of 86.4% were obtained in the detection of bilateral asymmetry.

The presence of bilateral asymmetry has been shown to be an important predictor of breast cancer [100]. More methods are desirable in this area to analyze asymmetry from multiple perspectives, including pattern asymmetry in the fibroglandular tissue as well as morphological and density measures related to the breast and the fibroglandular disk.

3.7. Detection of architectural distortion

Architectural distortion is one of the most commonly missed abnormalities in screening mammography. Architectural distortion is defined as distortion of the normal architecture

with no definite mass visible, including spiculations radiating from a point and focal retraction or distortion at the edge of the parenchyma [12]. The nonspecific definition of distortion and its subtle nature make the development of image processing techniques for its detection a challenge.

Sampat et al. [101] employed filtering in the Radon-transform domain to enhance mammograms, followed by the use of radial spiculation filters to detect spiculated lesions. The algorithm was tested on 45 cases exhibiting spiculated masses, and 45 cases with the presence of architectural distortion. A sensitivity of 80% was obtained at 14 false positives per image in the detection of architectural distortion, and 91% at 12 false positives per image in the detection of spiculated masses.

The use of fractal dimension to characterize the presence of architectural distortion in mammographic ROIs has been explored recently. Guo et al. [102] investigated the characterization of architectural distortion using the Hausdorff dimension, and a support vector machine classifier to distinguish between mammographic ROIs exhibiting architectural distortion and those with normal mammographic patterns. A set of 40 ROIs was selected from the MIAS database [73] (19 ROIs with architectural distortion and 21 ROIs with normal tissue patterns). The authors reported a classification accuracy of 72.5%. Tourassi et al. [103] studied the use of fractal dimension to differentiate between normal and architectural distortion patterns in mammographic ROIs. The dataset used in the investigation contained 112 ROIs with architectural distortion patterns, and 1388 ROIs exhibiting normal tissue patterns. An area under the ROC curve of $A_z = 0.89$ was obtained. The authors also reported that the average fractal dimension of ROIs exhibiting architectural distortion was observed to be lower than that of ROIs with normal patterns, and that the observed difference was statistically significant under an independent-sample, two-tailed t-test.

Matsubara et al. [104] used mathematical morphology to detect architectural distortion around the skin line, and a concentration index to detect architectural distortion within the mammary gland; the authors reported a sensitivity of 94% with 2.3 false positives per image, and 84% with 2.4 false positives per image, respectively. In a later report from the same research group, Ichikawa et al. [105] presented a method to detect architectural distortion that encompasses the detection of linear structures using the mean curvature of the image, the computation of a concentration index that indicates the presence of stellate structures over half-circles, and the detection of architectural distortion based on a set of local features that includes the concentration index; the authors reported a sensitivity of 68% with 3.4 false positives per image. Mudigonda and Rangayyan [106] proposed the use of texture flow-field to detect architectural distortion, based on the local coherence of texture orientation; only preliminary results were given, indicating the potential of the technique in the detection of architectural distortion.

Eltonsy et al. [107] proposed a method for the detection of masses and architectural distortion based on the identification of points surrounded by concentric layers of image activity. A test dataset of 80 images was used in the evaluation of the technique, containing 13 masses, 38 masses accompanied by architectural distortion, and 29 images exhibiting only architectural distortion. The authors reported an overall sensitivity of 91.3% with 9.1 false positives per image. A sensitivity of 93.1% in the detection of pure architectural distortion was also reported at the same level of false positives per image in the overall dataset.

Ayres and Rangayyan [108,109] studied the characterization of architectural distortion in mammographic ROIs using phase portraits. A phase portrait is a display of the possible trajectories, in the phase plane, of the state of a dynamical system. Rao and Jain [110] proposed the use of phase portraits in oriented texture analysis: the geometrical patterns in the phase portraits of systems of two linear, first-order, differential equations may be associated with the patterns encountered in an image presenting oriented texture. A database of 106 ROIs extracted from the Mini-MIAS database was used in the work of Ayres and Rangayyan [109], containing 17 cases of architectural distortion, 45 normals, two ROIs with malignant calcifications, and 44 masses (eight spiculated malignant, four circumscribed malignant, 11 spiculated benign, and 19 circumscribed benign masses). A sensitivity of 76.5% and a specificity of 76.4% were obtained, with an area under the ROC curve of $A_z = 0.77$.

Ayres and Rangayyan [111] extended their work to the detection of architectural distortion in full mammograms. Preliminary results indicated a sensitivity of 88% at a high false-positive rate of 15 false positives per image, with a dataset of 19 mammograms with architectural distortion, selected from the Mini-MIAS database. The mammograms are MLO views, digitized at a resolution of 200 μm and 8 bits/pixel. The inclusion of procedures to detect and reject confounding CLS led to improved results, with a sensitivity of 84% at 7.8 false positives per image [94,112]. Further improvement was obtained with the addition of a constraint to the phase portrait model that limited the range of possible phase portraits to those with orthogonal eigenvectors and limited singular-value ratio

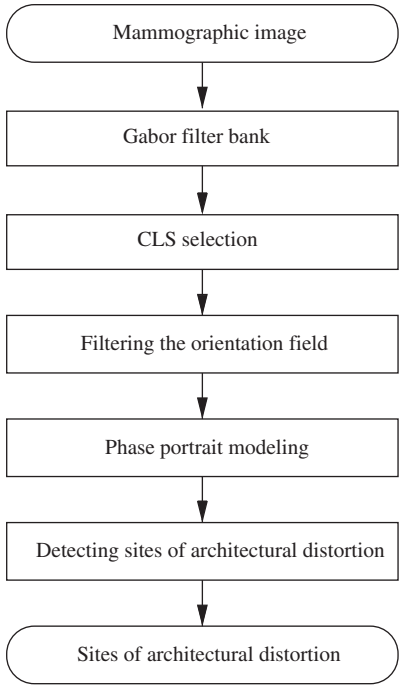

Fig. 8. Flowchart of the technique for the detection of architectural distortion in mammograms. CLS: curvilinear structure.

[113]; a sensitivity of 84% with 4.5 false positives per image was obtained, with a dataset of 19 images containing architectural distortion and 41 normal mammograms. Fig. 8 gives a flowchart of the technique for the detection of architectural distortion in mammograms [113]. The algorithm consists of the following steps:

(1) The oriented texture of the mammographic images is analyzed through the use of a Gabor filter bank, composed of several filters whose orientations span the range 0°–180°. The Gabor filter magnitude response and the best-fitting orientation are obtained at each pixel.
(2) The relevant CLS are extracted.
(3) The orientation field, composed of all the best-fitting orientations, is filtered and down sampled in order to reduce artifacts as well as the computational effort required by the subsequent steps. The filtering procedure employed is a variant of Rao and Jain's dominant local orientation method [110]: a Gaussian filter is used instead of a box filter. The detected CLS in the previous step are used as weighting factors in the filtering process, in order to emphasize the relevant oriented information and suppress confounding CLS.
(4) The filtered orientation field is processed to obtain the best local fit of a linear, first-order, shape-constrained phase portrait model. At each pixel, the parameters of the model are used to determine the type of the phase portrait that best describes the local orientation field (only node and saddle phase portraits are allowed due to the shape constraints in the model), and the location of the fixed point of the observed phase portrait. The information thus obtained is accumulated using a vote-casting procedure: two maps are created corresponding to the two allowed phase portrait types, and a vote is cast at the fixed point location, in the corresponding phase portrait map, for each pixel. The vote is not cast if the phase portrait model derived does not conform to the shape constraints.
(5) Detection and localization of sites of architectural distortion are performed using the node map.
    (a) A Gaussian filter of standard deviation equal to 4.8 mm is applied to the node map to reduce noise.
    (b) The filtered node map is processed with a morphological gray-scale opening procedure with a structuring element of radius 8 mm to eliminate peaks in the filtered node map that are closer than 8 mm to a locally dominant peak.
    (c) The peaks of the resulting image are detected, and a threshold is applied to eliminate false positives. The remaining peaks, if any, indicate the potential sites of architectural distortion.

Figs. 9–12 illustrate the results obtained at each step of the algorithm. The original mammogram is shown in Fig. 9; the location of architectural distortion (as given in the MIAS database [73]) is indicated by the white dashed circle. The magnitude response of the Gabor filters and the filtered orientation field images are shown in Figs. 10 and 11, respectively. It can be observed in Fig. 11 that the oriented texture of the breast image has a coherent direction in most of the breast area (excluding the pectoral muscle edge), except at and around the site of architectural distortion. At the site of architectural distortion, the orientation field does not present the regular appearance observed in the other areas of the breast, but forms a noticeable pattern of converging lines. (Such a pattern can also be

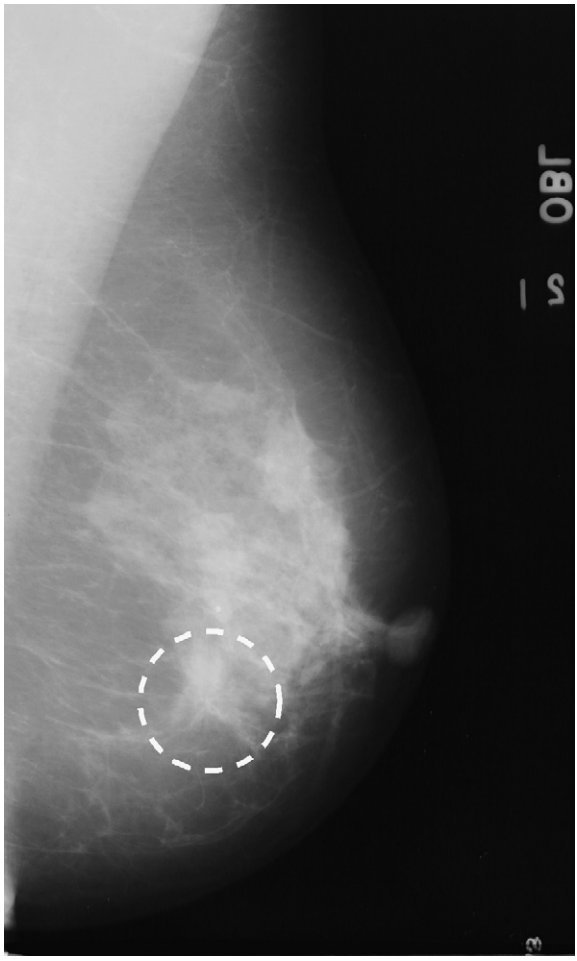

Fig. 9. Mammogram with architectural distortion (dashed circle). The image 'mdb120' from the Mini-MIAS database [73] is shown, with a pixel resolution of 200 μm per pixel.

noticed in the Gabor magnitude image in Fig. 10.) Fig. 12 shows the processed node map, where it can be observed that a high response is present at the site of architectural distortion, which was correctly detected.

A summary of selected methods for the detection of architectural distortion is given in Table 4. There is a need for further methods for objective characterization of the subtle and diverse patterns associated with architectural distortion from the perspectives of image processing and computer vision. We surmise that methods designed exclusively for the detection of architectural distortion can achieve better performance than the application of methods for the detection of spiculated masses, which may rely on the presence of a central mass. Accurate detection of architectural distortion could be the key to efficient detection of early breast cancer, at pre-mass-formation stages.

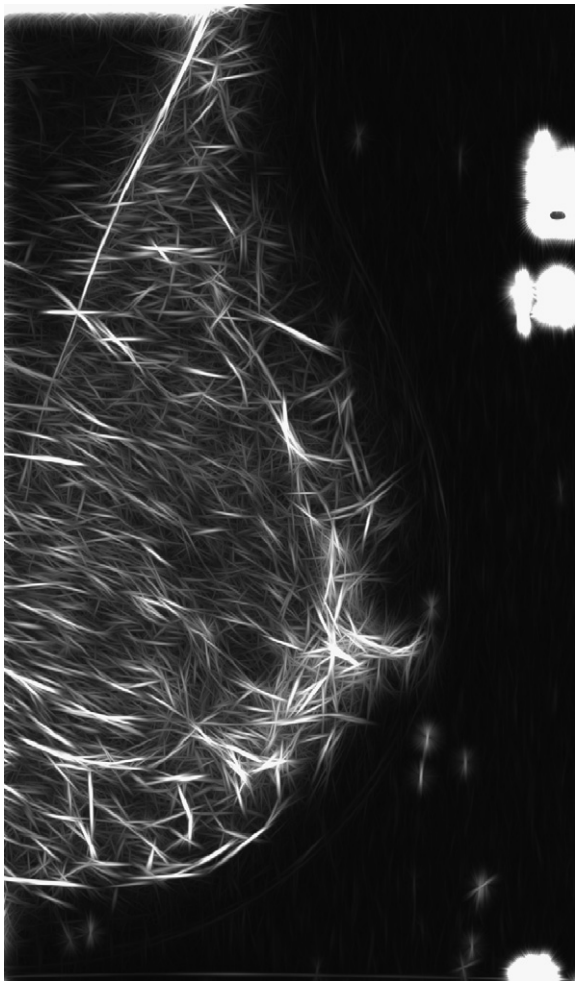

Fig. 10. Magnitude image produced by Gabor filtering. The original mammogram is shown in Fig. 9. Pixel resolution is 200 μm per pixel.

3.8. Analysis of prior mammograms

Screening mammography has a limited sensitivity [9], and it has been observed that subtle signs of abnormality can be seen in a significant fraction of previous screening mammograms of screen-detected or interval cases of breast cancer [10], hereafter referred to as prior mammograms. It is possible that such cases of missed signs of abnormality present indistinct, subtle, or hard-to-detect features related to early signs of breast cancer. Based on these observations, a few researchers have analyzed prior mammograms in efforts to improve the detection of early signs of breast cancer.

Sameti et al. [114] studied the structural differences between the regions that subsequently developed malignant masses on mammograms, and other normal areas in

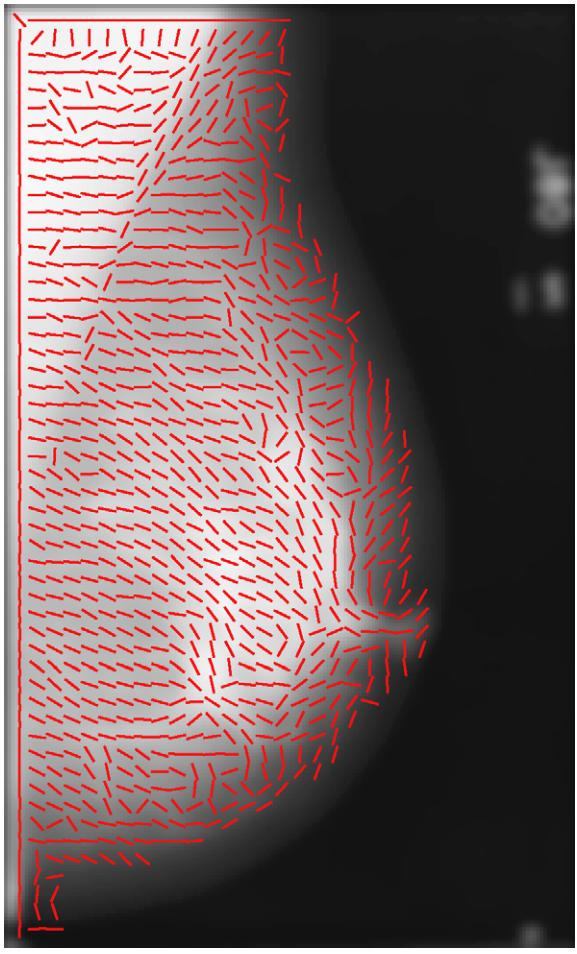

Fig. 11. Orientation field superimposed on the mammogram. The original mammogram is shown in Fig. 9. Pixel resolution is 200 μm per pixel. Needles are drawn only for pixels at every 10th row and 10th column.

images taken in the last screening instance prior to the detection of tumors. Manually identified circular ROIs were transformed into their optical-density equivalents, and further divided into three types of regions representing low, medium, and high optical density. Based upon the regions, a set of photometric and texture features was extracted. It was reported that in 72% of the 58 breast cancer cases studied, it was possible to realize the differences between malignant tumor regions and normal tissues in previous screening images.

Petrick et al. [115] studied the effectiveness of their mass-detection method in the detection of masses in prior mammograms. The dataset used included 92 images (54 malignant and 38 benign) from 37 cases (22 malignant and 15 benign). Their detection methods achieved a "by film" mass-detection sensitivity of 51% with 2.3 false positives per image; a slightly better accuracy of 57% was achieved in detecting only malignant tumors. The detection scheme of Petrick et al. attempts to segment salient densities by employing

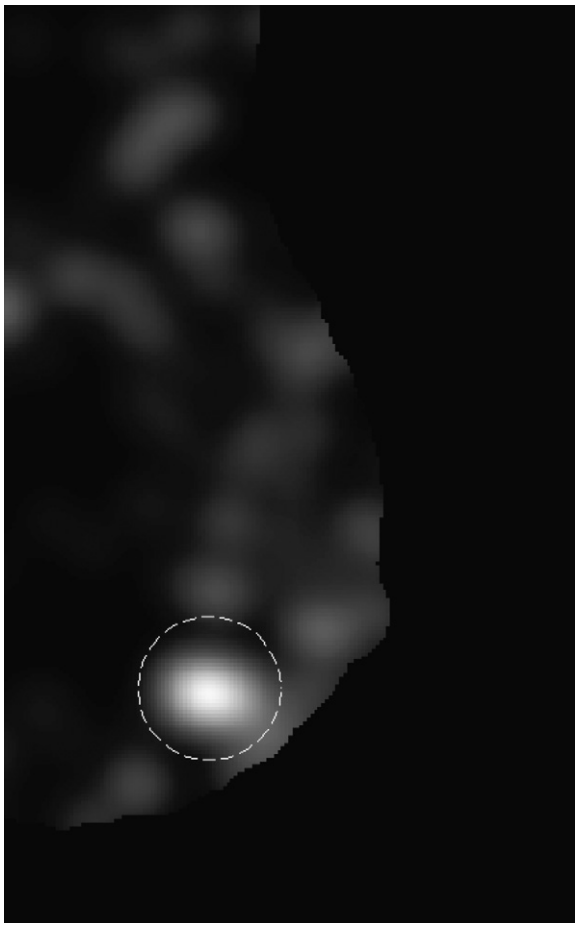

Fig. 12. Node map: the dashed circle indicates the site of architectural distortion. The original mammogram is shown in Fig. 9. Pixel resolution is 800 μm per pixel.

region growing after enhancement of contrast in the image. Such an intensity-based segmentation approach fails to detect the developing densities in prior mammograms due to the inadequate contrast of potentially abnormal regions before the masses are actually formed.

Zheng et al. [116] investigated the performance of a CAD algorithm for the detection of masses in current and prior mammograms in two scenarios: when the algorithm was optimized with current mammograms, and when the algorithm was optimized with prior mammograms. The CAD algorithm consisted of three steps: difference-of-Gaussian filtering and thresholding for the initial selection of potential lesion sites; adaptive region growing and topological analysis of the suspicious regions to eliminate false positives; and feature extraction (including shape, histogram, and texture features) and classification using an artificial neural network (ANN). A database of 260 pairs of consecutive mammograms was used in this work, where the latest image showed one or two masses, and the prior image had been originally classified as negative or probably benign. The first

Table 4
Performance statistics of selected CAD methods for the detection of architectural distortion

Authors	Size of dataset	Summary of results
Sampat et al. [101]	45 cases exhibiting spiculated masses, and 45 cases with the presence of architectural distortion	Sensitivity of 80% at 14 false positives per image
Guo et al. [102]	40 ROIs (19 ROIs with architectural distortion and 21 ROIs with normal tissue patterns)	Classification accuracy of 72.5%
Tourassi et al. [103]	112 ROIs with architectural distortion patterns, and 1,388 ROIs exhibiting normal tissue patterns	$A_z = 0.89$
Matsubara et al. [104]	55 mammograms exhibiting architectural distortion (17 with focal retraction, 38 with architectural distortion within the fibroglandular disk)	Detection of architectural distortion around the skinline: sensitivity of 94% with 2.3 false positives per image. Detection of architectural distortion within the fibroglandular disk: sensitivity of 84% with 2.4 false positives per image
Ichikawa et al. [105]	94 mammograms exhibiting architectural distortion	Sensitivity of 68% with 3.4 false positives per image
Eltonsy et al. [107]	80 images (13 masses, 38 masses accompanied by architectural distortion, and 29 images exhibiting only architectural distortion)	Overall sensitivity of 91.3% with 9.1 false positives per image. Sensitivity of 93.1% in the detection of pure architectural distortion
Ayres and Rangayyan [108,109]	106 ROIs (17 cases of architectural distortion, 45 normals, two ROIs with malignant calcifications, and 44 masses—eight spiculated malignant, four circumscribed malignant, 11 spiculated benign, and 19 circumscribed benign masses)	Sensitivity of 76.5% and specificity of 76.4%, $A_z = 0.77$
Ayres and Rangayyan [111]	19 mammograms with architectural distortion	Sensitivity of 88% at 15 false positives per image
Ayres and Rangayyan [94,112]	19 mammograms with architectural distortion	Sensitivity of 84% at 7.8 false positives per image
Rangayyan and Ayres [113]	19 images containing architectural distortion and 41 normal mammograms	Sensitivity of 84% at 4.5 false positives per image

Only works with ROC analysis and/or pattern classification results are listed.

two steps of the CAD algorithm were applied to both the current and prior images of the database, producing a set of 1,449 suspicious ROIs, which were classified according to the true mass location in the current mammograms. The ROIs were classified into the normal and mass categories using the third step of the CAD algorithm (feature extraction and ANN classification). The authors reported that training the ANN with the current mammograms resulted in areas under the ROC curves of 0.89 ± 0.01 and 0.65 ± 0.02 when classifying ROIs from the current and prior mammograms, respectively. When the ANN was trained with ROIs from the prior mammograms, areas under the ROC curve of

0.81 ± 0.02 and 0.71 ± 0.02 were obtained in the classification of ROIs from the current and prior mammograms, respectively. The results indicate the importance of developing CAD algorithms that incorporate knowledge about particular features of early signs, as opposed to the application of methods designed for well-developed masses, for the detection of early signs of breast cancer.

Burnside et al. [117] analyzed the impact of the availability of prior mammograms on the clinical outcomes of diagnostic and screening mammography. The authors concluded that comparison with previous mammograms significantly improves the specificity but not the sensitivity of screening mammography, and increases the sensitivity of diagnostic mammography. Ciatto et al. [118] compared single, double, and CAD-assisted reading of negative prior (screening) mammograms in interval-cancer cases. It was observed that CAD-assisted reading was almost as sensitive as double reading, and significantly more specific.

Simultaneous analysis of current and prior mammograms could improve the performance of radiologists in the detection of breast cancer, and may also enhance the performance of CAD systems in the same task.

3.9. *Full-field digital mammography*

Full-field digital mammography, although not a CAD technology in strict terms, has several advantageous features that can be explored by a CAD system. In a digital imaging system, the steps of image acquisition, processing, display, and storage are decoupled, allowing the optimization of each of these procedures. Several authors have presented reviews of current technologies in full-field digital mammography, e.g., James [119], Pisano [120], and Yaffe [121]. Lewin et al. [122] compared the performance of full-field digital mammography and screen-film mammography for the detection of breast cancer in a screening population. It was observed that no statistically significant difference ($p > 0.1$) existed in cancer detection, and that digital mammography resulted in fewer recalls than screen-film mammography ($p < 0.001$).

3.10. *Indexed atlases, data mining, and content-based retrieval*

The advent of mammographic screening programs has generated a variety of data, such as patient reports and mammographic images, stored in many databases across health centers and universities around the world. Such a wealth of data could be explored through the use of information management technologies, benefiting researchers, clinical practitioners, students, patients, companies engaged in research and development related to CAD systems, and other participants in the effort to reduce breast cancer mortality.

The Merriam-Webster dictionary defines data as "factual information (as measurements or statistics) used as a basis for reasoning, discussion, or calculation", and information as "knowledge obtained from investigation, study, or instruction". Data represent a meaningless entity that is transformed into information through the process of analysis and attribution of meaning. It is necessary to develop the proper computational tools in order to obtain useful information from the vast amounts of data present in mammographic and associated databases.

One can contemplate upon the usefulness of efficiently retrieving and analyzing information, by observing how search engines help in taming the massive complexity and

quantity of data available on the Internet. Nevertheless, it is necessary to tailor the information retrieval tools to the nature of the information being retrieved. Some researchers have investigated the application of content-based image retrieval (CBIR) and data mining techniques to explore the richness present in databases of mammograms and patient information [123]. Honda et al. [124] presented a CBIR system based on textural features and PCA: the authors reported a precision rate between 25% and 100%. Nakagawa et al. [125] presented a technique for CBIR where mammographic ROIs containing masses were represented by autocorrelation measures. The authors observed that the technique allowed the retrieval of ROIs that were visually similar to a given ROI, used as a query sample. Nevertheless, the visual similarity did not imply an agreement between the radiologist's assessment of the query ROI and the retrieved ROIs: an agreement of 29% was obtained in the shape of the mass, and 34% in the description of the mass border.

Alto et al. [126] investigated the suitability of objective measures of shape, edge sharpness, and texture to retrieve mammograms with masses having similar features. A measure of retrieval accuracy known as precision was determined to be 91% when using the three most-effective features investigated by the authors, namely fractional concavity, acutance, and sum entropy (a texture measure defined by Haralick [65]). Fig. 3 illustrates the process of feature extraction for a macrolobulated benign mass. The ROI of the mass is shown in Fig. 3a. Fig. 3b displays the contour of the mass, with concave parts in black and convex parts in white: fractional concavity is the fractional length of the concave segments to the total length of the contour. Fig. 3c shows the ribbon of pixels at the boundary of the mass used to compute texture measures. Fig. 3d exhibits a set of line segments (in black) perpendicular to the contour of the mass: the image intensity along these perpendicular line segments is used to compute acutance, a measure of edge sharpness. The results of the retrieval operation for a malignant tumor are illustrated in Fig. 13.

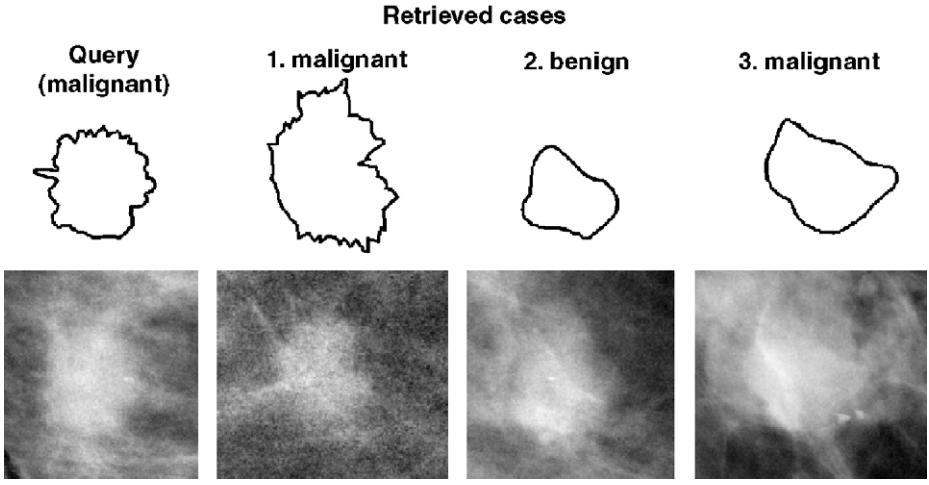

Fig. 13. Content-based retrieval with a microlobulated malignant tumor query sample using the three features fractional concavity (shape), acutance (edge sharpness), and sum entropy (texture measure). In each case, the gray-scale ROI and the corresponding contour drawn by a radiologist are shown. The top three matches selected from the database are shown.

Alto et al. [127] discuss several issues related to an effective design of an indexed atlas of digital mammograms for CAD of breast cancer. In particular, the use of objective measures derived by the application of image processing techniques to represent diagnostic features in mammograms could lead to semantic indexing, data mining, content-based retrieval, and comparative analysis of cases. Indexed atlases can be developed to help in the teaching and training of radiologists, and combined with content-based retrieval tools to help radiologists in the decision-making process for difficult-to-diagnose cases [128].

4. Concluding remarks

Breast cancer is the most common type of cancer in women. Early diagnosis is a fundamental requirement in order to achieve a reduction in mortality rates. Screening programs have contributed to a substantial reduction in mortality rates through early detection of the disease. Nevertheless, the complexity of mammograms and the high volume of exams per radiologist in a screening program continue to result in a significant number of errors; the errors can be reduced with double reading, an effective but costly measure. Computer-aided diagnosis technology offers an affordable alternative to double reading, and many studies indicate that CAD is effective in reducing the errors in mammographic screening to a level comparable to that achieved with double reading.

Many techniques have been established for the detection of masses and calcifications. Further developments are required to improve the detection of subtle signs of breast cancer, such as bilateral asymmetry and architectural distortion, in order to enable efficient and early detection of breast cancer.

Acknowledgment

This work was supported by the Natural Sciences and Engineering Research Council of Canada and the Alberta Heritage Foundation for Medical Research.

References

[1] National Cancer Institute of Canada, Canadian cancer statistics 2006, available at 〈http://www.cancer.ca/vgn/images/portal/cit_86751114/31/21/935505792cw_2006stats_en.pdf.pdf〉, accessed on June 1st, 2006.
[2] A. Jemal, L.X. Clegg, E. Ward, L.A.G. Ries, X. Wu, P.M. Jamison, P.A. Wingo, H.L. Howe, R.N. Anderson, B.K. Edwards, Annual report to the nation on the status of cancer, 1975–2001, with a special feature regarding survival, Cancer 101 (1) (2004) 3–27.
[3] C.D. Maggio, State of the art of current modalities for the diagnosis of breast lesions, Eur. J. Nucl. Med. Mol. Imaging 31 (Suppl. 1) (2004) S56–S69.
[4] A.K. Hackshaw, E.A. Paul, Breast self-examination and death from breast cancer: a meta-analysis, Br. J. Cancer 88 (2003) 1047–1053.
[5] M.J. Homer, Mammographic Interpretation: A Practical Approach, second ed., McGraw-Hill, New York, 1997.
[6] M.A. Schneider, Better detection: improving our chances, in: M.J. Yaffe (Ed.), Digital Mammography: Fifth International Workshop on Digital Mammography, Medical Physics Publishing, Toronto, ON, Canada, 2000, pp. 3–6.
[7] S.H. Heywang-Köbrunner, I. Schreer, D.D. Dershaw, Diagnostic Breast Imaging: Mammography, Sonography, Magnetic Resonance Imaging, and Interventional Procedures, Thieme Medical Publishers, New York, 1997.
[8] B. Cady, M. Chung, Mammographic screening: no longer controversial, Am. J. Clin. Oncol. 28 (1) (2005) 1–4.

[9] R.E. Bird, T.W. Wallace, B.C. Yankaskas, Analysis of cancers missed at screening mammography, Radiology 184 (3) (1992) 613–617.
[10] J.A.A.M. van Dijck, A.L.M. Verbeek, J.H.C.L. Hendriks, R. Holland, The current detectability of breast cancer in a mammographic screening program, Cancer 72 (6) (1993) 1933–1938.
[11] R.G. Blanks, M.G. Wallis, S.M. Moss, A comparison of cancer detection rates achieved by breast cancer screening programmes by number of readers, for one and two view mammography: Results from the UK National Health Service Breast Screening Programme, J. Med. Screening 5 (4) (1998) 195–201.
[12] American College of Radiology (ACR), Illustrated Breast Imaging Reporting and Data System (BI-RADS), third ed., American College of Radiology, Reston, VA, 1998.
[13] E.A. Sickles, Mammographic features of 300 consecutive nonpalpable breast cancers, Am. J. Roentgenol. 146 (4) (1986) 661–663.
[14] H.C. Burrell, D.M. Sibbering, A.R.M. Wilson, S.E. Pinder, A.J. Evans, L.J. Yeoman, C.W. Elston, I.O. Ellis, R.W. Blamey, J.F.R. Robertson, Screening interval breast cancers: mammographic features and prognostic factors, Radiology 199 (4) (1996) 811–817.
[15] R2 Technology website, 〈http://www.r2tech.com/〉, accessed on March 6, 2005.
[16] iCAD website, 〈http://www.icadmed.com/〉, accessed on March 6, 2005.
[17] S.M. Astley, F.J. Gilbert, Computer-aided detection in mammography, Clin. Radiol. 59 (2004) 390–399.
[18] S. Ciatto, M.R.D. Turco, G. Risso, S. Catarzi, R. Bonaldi, V. Viterbo, P. Gnutti, B. Guglielmoni, L. Pinelli, A. Pandiscia, F. Navarra, A. Lauria, R. Palmiero, P.L. Indovina, Comparison of standard reading and computer aided detection (CAD) on a national proficiency test of screening mammography, Eur. J. Radiol. 45 (2003) 135–138.
[19] T.W. Freer, M.J. Ulissey, Screening mammography with computer-aided detection: Prospective study of 12,860 patients in a community breast center, Radiology 220 (2001) 781–786.
[20] L.J.W. Burhenne, S.A. Wood, C.J. D'Orsi, S.A. Feig, D.B. Kopans, L.F. O'Shaughnessy, E.A. Sickles, L. Tabar, C.J. Vyborny, R.A. Castellino, Potential contribution of computer-aided detection to the sensitivity of screening mammography, Radiology 215 (2) (2000) 554–562.
[21] W.P. Evans, L.J.W. Burhenne, L. Laurie, K.F. O'Shaughnessy, R.A. Castellino, Invasive lobular carcinoma of the breast: Mammographic characteristics and computer-aided detection, Radiology 225 (1) (2002) 182–189.
[22] R.L. Birdwell, D.M. Ikeda, K.F. O'Shaughnessy, E.A. Sickles, Mammographic characteristics of 115 missed cancers later detected with screening mammography and the potential utility of computer-aided detection, Radiology 219 (1) (2001) 192–202.
[23] J.A. Baker, E.L. Rosen, J.Y. Lo, E.I. Gimenez, R. Walsh, M.S. Soo, Computer-aided detection (CAD) in screening mammography: Sensitivity of commercial CAD systems for detecting architectural distortion, Am. J. Roentgenol. 181 (2003) 1083–1088.
[24] M.J.M. Broeders, N.C. Onland-Moret, H.J.T.M. Rijken, J.H.C.L. Hendriks, A.L.M. Verbeek, R. Holland, Use of previous screening mammograms to identify features indicating cases that would have a possible gain in prognosis following earlier detection, Eur. J. Cancer 39 (12) (1993) 1770–1775.
[25] H.-O. Peitgen (Ed.), Proceedings of the Sixth International Workshop on Digital Mammography, Springer, Bremen, Germany, 2002.
[26] E. Pisano (Ed.), Proceedings of the Seventh International Workshop on Digital Mammography, Durham, NC, 2004.
[27] G. Ram, Optimization of ionizing radiation usage in medical imaging by means of image enhancement techniques, Med. Phys. 9 (5) (1982) 733–737.
[28] R.M. Rangayyan, Biomedical Image Analysis, CRC Press, Boca Raton, FL, 2005.
[29] W.M. Morrow, R.B. Paranjape, R.M. Rangayyan, J.E.L. Desautels, Region-based contrast enhancement of mammograms, IEEE Trans. Med. Imaging 11 (3) (1992) 392–406.
[30] R.M. Rangayyan, L. Shen, Y. Shen, J.E.L. Desautels, H. Bryant, T.J. Terry, N. Horeczko, M.S. Rose, Improvement of sensitivity of breast cancer diagnosis with adaptive neighborhood contrast enhancement of mammograms, IEEE Trans. Inform. Technol. Biomed. 1 (3) (1997) 161–170.
[31] H.P. Chan, C.J. Vyborny, H. MacMahon, C.E. Metz, K. Doi, E.A. Sickles, ROC studies of the effects of pixel size and unsharp-mask filtering on the detection of subtle microcalcifications, Invest. Radiol. 22 (1987) 581–589.
[32] A.F. Laine, S. Schuler, J. Fan, W. Huda, Mammographic feature enhancement by multiscale analysis, IEEE Trans. Med. Imaging 13 (4) (1994) 725–740.

[33] R. Gordon, R.M. Rangayyan, Feature enhancement of film mammograms using fixed and adaptive neighborhoods, Appl. Opt. 23 (4) (1984) 560–564.
[34] R.M. Rangayyan, H.N. Nguyen, Pixel-independent image processing techniques for noise removal and feature enhancement, in: IEEE Pacific Rim Conference on Communications, Computers, and Signal Processing, IEEE, Vancouver, BC, Canada, 1987, pp. 81–84.
[35] A.P. Dhawan, G. Buelloni, R. Gordon, Enhancement of mammographic features by optimal adaptive neighborhood image processing, IEEE Trans. Med. Imaging 5 (1) (1986) 8–15.
[36] A.P. Dhawan, E. Le Royer, Mammographic feature enhancement by computerized image processing, Comput. Methods Programs Biomed. 27 (1988) 23–35.
[37] C. Kimme-Smith, R.H. Gold, L.W. Bassett, L. Gormley, C. Morioka, Diagnosis of breast calcifications: comparison of contact, magnified, and television-enhanced images, Am. J. Roentgenol. 153 (1989) 963–967.
[38] R.M. Rangayyan, L. Shen, Y. Shen, M.S. Rose, J.E.L. Desautels, H.E. Bryant, T.J. Terry, N. Horeczko, Region-based contrast enhancement, in: R.N. Strickland (Ed.), Image-Processing Techniques for Tumor Detection, Marcel Dekker, New York, 2002, pp. 213–242.
[39] R. Sivaramakrishna, N.A. Obuchowski, W.A. Chilcote, G. Cardenosa, K.A. Powell, Comparing the performance of mammographic enhancement algorithms—a preference study, Am. J. Roentgenol. 175 (2000) 45–51.
[40] T.-L. Ji, M.K. Sundareshan, H. Roehrig, Adaptive image contrast enhancement based on human visual properties, IEEE Trans. Med. Imaging 13 (4) (1994) 573–586.
[41] S.M. Pizer, E.P. Amburn, J.D. Austin, R. Cromartie, A. Geselowitz, T. Geer, B. ter Haar Romeny, J.B. Zimmerman, K. Zuiderveld, Adaptive histogram equalization and its variations, Comput. Vis. Graphics Image Process. 39 (1987) 355–368.
[42] A. Laine, J. Fan, W.H. Yan, Wavelets for contrast enhancement of digital mammography, IEEE Eng. Med. Biol. Mag. 14 (5) (1995) 536–550.
[43] N.F. Boyd, J.W. Byng, R.A. Jong, E.K. Fishell, L.E. Little, A.B. Miller, G.A. Lockwood, D.L. Tritchler, M.J. Yaffe, Quantitative classification of mammographic densities and breast cancer risk: results from the Canadian National Breast Screening Study, J. Nat. Cancer Inst. 87 (9) (1995) 670–675.
[44] G. Ursin, L. Hovanessian-Larsen, Y. Parisky, M.C. Pike, A.W. A, Greatly increased occurrence of breast cancers in areas of mammographically dense tissue, Breast Cancer Res. 7 (2005) R605–R608.
[45] J.W. Byng, N.F. Boyd, E. Fishell, R.A. Jong, M.J. Yaffe, Automated analysis of mammographic densities, Phys. Med. Biol. 41 (1996) 909–923.
[46] S. Caulkin, S. Astley, J. Asquith, C. Boggis, Sites of occurrence of malignancies in mammograms, in: N. Karssemeijer, M. Thijssen, J. Hendriks, L. van Erning (Eds.), Proceedings of the Fourth International Workshop on Digital Mammography, Nijmegen, The Netherlands, 1998, pp. 279–282.
[47] N. Karssemeijer, Automated classification of parenchymal patterns in mammograms, Phys. Med. Biol. 43 (2) (1998) 365–378.
[48] R.J. Ferrari, R.M. Rangayyan, J.E.L. Desautels, R.A. Borges, A.F. Frère, Automatic identification of the pectoral muscle in mammograms, IEEE Trans. Med. Imaging 23 (2004) 232–245.
[49] P.K. Saha, J.K. Udupa, E.F. Conant, D.P. Chakraborty, D. Sullivan, Breast tissue density quantification via digitized mammograms, IEEE Trans. Med. Imaging 20 (8) (2001) 792–803.
[50] Y. Sun, J. Suri, J. Desautels, R. Rangayyan, A new approach for breast skin-line estimation in mammograms, Pattern Anal. Appl. 9 (2006) 34–47.
[51] R.J. Ferrari, R.M. Rangayyan, J.E.L. Desautels, R.A. Borges, A.F. Frère, Identification of the breast boundary in mammograms using active contour models, Med. Biol. Eng. Comput. 42 (2004) 201–208.
[52] R.J. Ferrari, R.M. Rangayyan, R.A. Borges, A.F. Frère, Segmentation of the fibro-glandular disc in mammograms using Gaussian mixture modeling, Med. Biol. Eng. Comput. 42 (2004) 378–387.
[53] S.A. Feig, B.M. Galkin, H.D. Muir, Evaluation of breast microcalcifications by means of optically magnified tissue specimen radiographs, in: S. Bruñner, B. Langfeldt (Eds.), Recent Results in Cancer Research, vol. 105, Springer, Berlin, Germany, 1987, pp. 111–123.
[54] E.A. Sickles, Breast calcifications: mammographic evaluation, Radiology 160 (1986) 289–293.
[55] H.D. Cheng, X. Cai, X. Chen, L. Hu, X. Lou, Computer-aided detection and classification of microcalcifications in mammograms: a survey, Pattern Recogn. 36 (2003) 2967–2991.
[56] L. Shen, R.M. Rangayyan, J.E.L. Desautels, Detection and classification of mammographic calcifications, Int. J. Pattern Recogn. Artif. Intell. 7 (6) (1993) 1403–1416.
[57] L. Shen, R.M. Rangayyan, J.E.L. Desautels, Application of shape analysis to mammographic calcifications, IEEE Trans. Med. Imaging 13 (2) (1994) 263–274.

[58] I.N. Bankman, T. Nizialek, I. Simon, O.B. Gatewood, I.N. Weinberg, W.R. Broody, Segmentation algorithms for detecting microcalcifications in mammograms, IEEE Trans. Inform. Technol. Biomed. 1 (2) (1997) 141–149.
[59] R.N. Strickland, Wavelet transforms for detecting microcalcifications in mammograms, IEEE Trans. Med. Imaging 15 (2) (1996) 218–229.
[60] I. El-Naqa, Y. Yang, M.N. Wernick, N.P. Galatsanos, R.M. Nishikawa, A support vector machine approach for detection of microcalcifications, IEEE Trans. Med. Imaging 21 (12) (2002) 1552–1563.
[61] L. Wei, Y. Yang, R.M. Nishikawa, M.N. Vernick, A. Edwards, Relevance vector machine for automatic detection of clustered microcalcifications, IEEE Trans. Med. Imaging 24 (10) (2005) 1278–1285.
[62] S.-N. Yu, K.-Y. Li, Y.-K. Huang, Detection of microcalcifications in digital mammograms using wavelet filter and Markov random field model, Comput. Med. Imaging Graphics 30 (2006) 163–173.
[63] S. Yu, L. Guan, A CAD system for the automatic detection of clustered microcalcifications in digitized mammogram films, IEEE Trans. Med. Imaging 19 (2) (2000) 115–126.
[64] H. Soltanian-Zadeh, F. Rafiee-Rad, S. Pourabdollah-Nejad, Comparison of multiwavelet, wavelet, Haralick, and shape features for microcalcification classification in mammograms, Pattern Recogn. 37 (2004) 1973–1986.
[65] R.M. Haralick, Statistical and structural approaches to texture, Proc. IEEE 67 (1979) 786–804.
[66] C. Serrano, J.D. Trujillo, B. Acha, R.M. Rangayyan, Use of 2D linear prediction error to detect microcalcifications in mammograms, in: CDROM, Proceedings of the II Latin American Congress on Biomedical Engineering, Havana, Cuba, 2001.
[67] B. Acha, C. Serrano, R.M. Rangayyan, J.E.L. Desautels, Detection of microcalcifications in mammograms, in: J.S. Suri, R.M. Rangayyan (Eds.), Recent Advances in Breast Imaging, Mammography, and Computer-Aided Diagnosis of Breast Cancer, SPIE, Bellingham, WA, 2006, pp. 291–314 (Chapter 9).
[68] G.R. Kuduvalli, R.M. Rangayyan, Performance analysis of reversible image compression techniques for high-resolution digital teleradiology, IEEE Trans. Med. Imaging 11 (3) (1992) 430–445.
[69] D. Brzakovic, X.M. Luo, P. Brzakovic, An approach to automated detection of tumors in mammograms, IEEE Trans. Med. Imaging 9 (3) (1990) 233–241.
[70] W.P. Kegelmeyer Jr., J.M. Pruneda, P.D. Bourland, A. Hillis, M.W. Riggs, M.L. Nipper, Computer-aided mammographic screening for spiculated lesions, Radiology 191 (2) (1994) 331–337.
[71] K.I. Laws, Rapid texture identification, in: Proceedings of SPIE: Image Processing for Missile Guidance, vol. 238, 1980, pp. 376–380.
[72] N. Karssemeijer, G.M. te Brake, Detection of stellate distortions in mammograms, IEEE Trans. Med. Imaging 15 (5) (1996) 611–619.
[73] J. Suckling, J. Parker, D.R. Dance, S. Astley, I. Hutt, C.R.M. Boggis, I. Ricketts, E. Stamakis, N. Cerneaz, S.-L. Kok, P. Taylor, D. Betal, J. Savage, The Mammographic Image Analysis Society Digital Mammogram Database, in: A.G. Gale, S.M. Astley, D.D. Dance, A.Y. Cairns (Eds.), Digital Mammography: Proceedings of the 2nd International Workshop on Digital Mammography, Elsevier, York, UK, 1994, pp. 375–378.
[74] G.M. te Brake, N. Karssemeijer, Single and multiscale detection of masses in digital mammograms, IEEE Trans. Med. Imaging 18 (7) (1999) 628–639.
[75] R.M. Rangayyan, N.R. Mudigonda, J.E.L. Desautels, Boundary modelling and shape analysis methods for classification of mammographic masses, Med. Biol. Eng. Comput. 38 (2000) 487–496.
[76] B.S. Sahiner, H.P. Chan, N. Petrick, M.A. Helvie, L.M. Hadjiiski, Improvement of mammographic mass characterization using spiculation measures and morphological features, Med. Phys. 28 (7) (2001) 1455–1465.
[77] B.S. Sahiner, H.P. Chan, N. Petrick, M.A. Helvie, M.M. Goodsitt, Computerized characterization of masses on mammograms: The rubber band straightening transform and texture analysis, Med. Phys. 25 (4) (1998) 516–526.
[78] N.R. Mudigonda, R.M. Rangayyan, J.E.L. Desautels, Gradient and texture analysis for the classification of mammographic masses, IEEE Trans. Med. Imaging 19 (10) (2000) 1032–1043.
[79] N.R. Mudigonda, R.M. Rangayyan, J.E.L. Desautels, Detection of breast masses in mammograms by density slicing and texture flow-field analysis, IEEE Trans. Med. Imaging 20 (12) (2001) 1215–1227.
[80] R.M. Rangayyan, N.M. El-Faramawy, J.E.L. Desautels, O.A. Alim, Measures of acutance and shape for classification of breast tumors, IEEE Trans. Med. Imaging 16 (6) (1997) 799–810.
[81] L. Li, R.A. Clark, J.A. Thomas, Computer-aided diagnosis of masses with full-field digital mammography, Acad. Radiol. 9 (2002) 4–12.

[82] L. Zheng, A.K. Chan, An artificial intelligent algorithm for tumor detection in screening mammogram, IEEE Trans. Med. Imaging 20 (7) (2001) 559–567.
[83] S. Liu, C.F. Babbs, E.J. Delp, Multiresolution detection of spiculated lesions in digital mammograms, IEEE Trans. Image Process. 10 (6) (2001) 874–884.
[84] R. Zwiggelaar, T.C. Parr, I.W. Hutt, C.J. Taylor, S.M. Astley, C.R.M. Boggis, Model-based detection of spiculated lesions in mammograms, Med. Image Anal. 3 (1) (1999) 39–63.
[85] D. Guliato, R.M. Rangayyan, W.A. Carnielli, J.A. Zuffo, J.E.L. Desautels, Segmentation of breast tumors in mammograms using fuzzy sets, J. Electron. Imaging 12 (3) (2003) 369–378.
[86] D. Guliato, R.M. Rangayyan, W.A. Carnielli, J.A. Zuffo, J.E.L. Desautels, Fuzzy fusion operators to combine results of complementary medical image segmentation techniques, J. Electron. Imaging 12 (3) (2003) 379–389.
[87] C. Evans, K. Yates, M. Brady, Statistical characterization of normal curvilinear structures in mammograms, in: H.-O. Peitgen (Ed.), Proceedings of the Sixth International Workshop on Digital Mammography (IWDM 2002), Springer, Bremen, Germany, 2002, pp. 285–291.
[88] L.C.C. Wai, M. Mellor, M. Brady, A multi-resolution CLS detection algorithm for mammographic image analysis, in: C. Barillot, D.R. Haynor, P. Hellier (Eds.), Lecture Notes in Computer Science, Proceedings of Medical Image Computing and Computer-Assisted Intervention (MICCAI 2004), Springer, Berlin, Germany, 2004, pp. 865–872.
[89] R. Zwiggelaar, S.M. Astley, C.R.M. Boggis, C.J. Taylor, Linear structures in mammographic images: detection and classification, IEEE Trans. Med. Imaging 23 (9) (2004) 1077–1086.
[90] R.N. Dixon, C.J. Taylor, Automated asbestos fibre counting, Inst. Phys. Conf. Ser. 44 (1979) 178–185.
[91] R. Zwiggelaar, T.C. Parr, C.J. Taylor, Finding orientated line patterns in digital mammographic images, in: Proceedings of the Seventh British Machine Vision Conference, Edinburgh, UK, 1996, pp. 715–724.
[92] W.T. Freeman, E.H. Adelson, The design and use of steerable filters, IEEE Trans. Pattern Anal. Mach. Intell. 13 (9) (1991) 891–906.
[93] T. Lindeberg, Edge detection and ridge detection with automatic scale selection, Int. J. Comput. Vis. 30 (2) (1998) 117–154.
[94] R.M. Rangayyan, F.J. Ayres, Detection of architectural distortion in mammograms using Gabor filters and phase portraits, Med. Biol. Eng. Comput. 44 (10) (2006) 883–894.
[95] P. Miller, S. Astley, Detection of breast asymmetry using anatomical features, in: R.S. Acharya, C.B. Goldgof (Eds.), Biomedical Image Processing and Biomedical Visualization, vol. 1905 of Proceedings of SPIE, SPIE, San Jose, CA, 1993, pp. 433–442.
[96] P. Miller, S. Astley, Automated detection of breast asymmetry using anatomical features, in: K.W. Bowyer, S. Astley (Eds.), State of the Art in Digital Mammographic Image Analysis, vol. 9 of Series in Machine Perception and Artificial Intelligence, World Scientific, River Edge, NJ, 1994, pp. 247–261.
[97] T.-K. Lau, W.F. Bischof, Automated detection of breast tumors using the asymmetry approach, Comput. Biomed. Res. 24 (1991) 273–295.
[98] R.J. Ferrari, R.M. Rangayyan, J.E.L. Desautels, A.F. Frère, Analysis of asymmetry in mammograms via directional filtering with Gabor wavelets, IEEE Trans. Med. Imaging 20 (9) (2001) 953–964.
[99] R.M. Rangayyan, R.J. Ferrari, A.F. Frère, Detection of asymmetry between left and right mammograms, in: E. Pisano (Ed.), Proceedings of the Seventh International Workshop on Digital Mammography, Durham, NC, 2004, pp. 651–658.
[100] D. Scutt, G.A. Lancaster, J.T. Manning, Breast asymmetry and predisposition to breast cancer, Breast Cancer Res. 8 (2006) R14 URL ⟨http://breast-cancer-research.com/content/8/2/R14⟩.
[101] M.P. Sampat, G.J. Whitman, M.K. Markey, A.C. Bovik, Evidence based detection of spiculated masses and architectural distortion, in: J.M. Fitzpatrick, J.M. Reinhardt (Eds.), Proceedings of SPIE Medical Imaging 2005: Image Processing, vol. 5747, San Diego, CA, 2005, pp. 26–37.
[102] Q. Guo, J. Shao, V. Ruiz, Investigation of support vector machine for the detection of architectural distortion in mammographic images, J. Phys.: Conf. Ser. 15 (2005) 88–94.
[103] G.D. Tourassi, D.M. Delong, C.E. Floyd Jr., A study on the computerized fractal analysis of architectural distortion in screening mammograms, Phys. Med. Biol. 51 (5) (2006) 1299–1312.
[104] T. Matsubara, T. Ichikawa, T. Hara, H. Fujita, S. Kasai, T. Endo, T. Iwase, Automated detection methods for architectural distortions around skinline and within mammary gland on mammograms, in: H.U. Lemke, M.W. Vannier, K. Inamura, A.G. Farman, K. Doi, J.H.C. Reiber (Eds.), International Congress Series: Proceedings of the 17th International Congress and Exhibition on Computer Assisted Radiology and Surgery, Elsevier, London, UK, 2003, pp. 950–955.

[105] T. Ichikawa, T. Matsubara, T. Hara, H. Fujita, T. Endo, T. Iwase, Automated detection method for architectural distortion areas on mammograms based on morphological processing and surface analysis, in: J.M. Fitzpatrick, M. Sonka (Eds.), Proceedings of SPIE Medical Imaging 2004: Image Processing, SPIE, San Diego, CA, 2004, pp. 920–925.
[106] N.R. Mudigonda, R.M. Rangayyan, Texture flow-field analysis for the detection of architectural distortion in mammograms, in: A.G. Ramakrishnan (Ed.), Proceedings of Biovision, Bangalore, India, 2001, pp. 76–81.
[107] N. Eltonsy, G. Tourassi, A. Elmaghraby, Investigating performance of a morphology-based CAD scheme in detecting architectural distortion in screening mammograms, in: H.U. Lemke, K. Inamura, K. Doi, M.W. Vannier, A.G. Farman (Eds.), Proceedings of the 20th International Congress and Exhibition on Computer Assisted Radiology and Surgery (CARS 2006), Springer, Osaka, Japan, 2006, pp. 336–338.
[108] F.J. Ayres, R.M. Rangayyan, Characterization of architectural distortion in mammograms, in: Proceedings of the 25th Annual International Conference of the IEEE Engineering in Medicine and Biology Society (CD-ROM), Cancún, Mexico, 2003, pp. 886–889.
[109] F.J. Ayres, R.M. Rangayyan, Characterization of architectural distortion in mammograms, IEEE Eng. Med. Biol. Mag. 24 (1) (2005) 59–67.
[110] A.R. Rao, R.C. Jain, Computerized flow field analysis: oriented texture fields, IEEE Trans. Pattern Anal. Mach. Intell. 14 (7) (1992) 693–709.
[111] F.J. Ayres, R.M. Rangayyan, Detection of architectural distortion in mammograms using phase portraits, in: J.M. Fitzpatrick, M. Sonka (Eds.), Proceedings of SPIE Medical Imaging 2004: Image Processing, vol. 5370, San Diego, CA, 2004, pp. 587–597.
[112] F.J. Ayres, R.M. Rangayyan, Detection of architectural distortion in mammograms via analysis of phase portraits and curvilinear structures, in: Proceedings of the Third European Medical and Biological Engineering Conference, IFMBE European Conference on Biomedical Engineering (CD-ROM), vol. 11, Prague, Czech Republic, 2005, paper number 1873, six pages on CD-ROM.
[113] R.M. Rangayyan, F.J. Ayres, Detection of architectural distortion in mammograms using a shape-constrained phase portrait model, in: H.U. Lemke, K. Inamura, K. Doi, M.W. Vannier, A.G. Farman (Eds.), Proceedings of the 20th International Congress and Exhibition on Computer Assisted Radiology and Surgery (CARS 2006), Springer, Osaka, Japan, 2006, pp. 334–336.
[114] M. Sameti, J. Morgan-Parkes, R.K. Ward, B. Palcic, Classifying image features in the last screening mammograms prior to detection of a malignant mass, in: N. Karssemeijer, M. Thijssen, J. Hendriks, L. van Erning, (Eds.), Proceedings of the Fourth International Workshop on Digital Mammography, Nijmegen, The Netherlands, 1998, pp. 127–134.
[115] N. Petrick, H.P. Chan, B. Sahiner, M.A. Helvie, S. Paquerault, Evaluation of an automated computer-aided diagnosis system for the detection of masses on prior mammograms, in: Proceedings of SPIE, Medical Imaging 2000: Image Processing, vol. 3979, 2000, pp. 967–973.
[116] B. Zheng, W.F. Good, D.R. Armfield, C. Cohen, T. Hertzberg, J.H. Sumkin, D. Gur, Performance change of mammographic CAD schemes optimized with most-recent and prior image databases, Acad. Radiol. 10 (2003) 283–288.
[117] E.S. Burnside, E.A. Sickles, R.E. Sohlich, K.E. Dee, Differential value of comparison with previous examinations in diagnostic versus screening mammography, Am. J. Roentgenol. 179 (2002) 1173–1177.
[118] S. Ciatto, M.R.D. Turco, P. Burke, C. Visioli, E. Paci, M. Zappa, Comparison of standard and double reading and computer-aided detection (CAD) of interval cancers at prior negative screening mammograms: blind review, Br. J. Cancer 89 (2003) 1645–1649.
[119] J.J. James, The current status of digital mammography, Clin. Radiol. 59 (2004) 1–10.
[120] E.D. Pisano, Current status of full-field digital mammography, Radiology 214 (2000) 26–28.
[121] M.J. Yaffe, Development of full field digital mammography, in: N. Karssemeijer, M. Thijssen, J. Hendriks, L. van Erning (Eds.), Digital Mammography, Kluwer Academic Publishers, Nijmegen, The Netherlands, 1998, pp. 3–10.
[122] J.M. Lewin, C.J. D'Orsi, R.E. Hendrick, L.J. Moss, P.K. Isaacs, A. Karellas, G.R. Cutter, Clinical comparison of full-field digital mammography and screen-film mammography for detection of breast cancer, Am. J. Roentgenol. 179 (2002) 671–677.
[123] X. Wang, M.R. Smith, R.M. Rangayyan, Mammographic information analysis through association-rule mining, in: Proceedings of the IEEE Canadian Conference on Electrical and Computer Engineering, Niagara Falls, ON, 2004, pp. 1495–1498.

[124] M.O. Honda, P.M. de Azevedo Marques, J.A.H. Rodrigues, Content-based image retrieval in mammography: using texture features for correlation with BI-RADS categories, in: H.-O. Peitgen (Ed.), Proceedings of the Sixth International Workshop on Digital Mammography: IWDM 2002, Springer, Bremen, Germany, 2002, pp. 231–233.

[125] T. Nakagawa, T. Hara, H. Fujita, T. Iwase, T. Endo, Image retrieval system of mammographic masses by using local pattern matching technique, in: H.-O. Peitgen (Ed.), Proceedings of the Sixth International Workshop on Digital Mammography: IWDM 2002, Springer, Bremen, Germany, 2002, pp. 562–565.

[126] H. Alto, R.M. Rangayyan, J.E.L. Desautels, Content-based retrieval and analysis of mammographic masses, J. Electron. Imaging 14 (2) (2005) 1–17.

[127] H. Alto, R.M. Rangayyan, R.B. Paranjape, J.E.L. Desautels, H. Bryant, An indexed atlas of digital mammograms for computer-aided diagnosis of breast cancer, Ann. Télécommun. 58 (5–6) (2003) 820–835.

[128] D. Guliato, E.V. de Melo, R.S. Bôaventura, R.M. Rangayyan, AMDI — indexed atlas of digital mammograms that integrates case studies, e-learning, and research systems via the web, in: J.S. Suri, R.M. Rangayyan (Eds.), Recent Advances in Breast Imaging, Mammography, and Computer-aided Diagnosis of Breast Cancer, SPIE Press, Bellingham, WA, 2006, pp. 529–555 (Chapter 15).